Theor Chem Acc (2010) 127:449–465
DOI 10.1007/s00214-010-0732-8

REGULAR ARTICLE

Transition metal oxide clusters with character of oxygen-centered radical: a DFT study

Yan-Xia Zhao · Xun-Lei Ding · Yan-Ping Ma · Zhe-Chen Wang · Sheng-Gui He

Received: 25 November 2009 / Accepted: 5 February 2010 / Published online: 25 February 2010

Abstract Density functional theory (DFT) calculations are applied to study the structure and bonding properties of groups 3–7 transition metal oxide clusters $M_{x=1-3}O_y^q$ and $Sc_{x=4-6}O_y^q$ with $2y - nx + q = 1$, in which n is the number of metal valence electrons and q is the charge number. These clusters include MO_2, $M_2O_3^+$, $M_2O_4^-$, and M_3O_5 (M = Sc, Y, La); MO_2^+, MO_3^-, $M_2O_4^+$, $M_2O_5^-$, $M_3O_6^+$, and $M_3O_7^-$ (M = Ti, Zr, Hf), and so on. The obtained lowest energy structures of most of these clusters are with character of oxygen-centered radical ($O^{\cdot}$). That is, the clusters contain oxygen atom(s) with the unpaired electron being localized on the 2p orbital(s). Chromium and manganese oxide clusters (except CrO_4^-) do not contain $O^{\cdot}$ with the adopted DFT methods. The binding energies of the radical oxygen with the clusters are also calculated. The DFT results are supported by available experimental investigations and predict that a lot of other transition metal oxide clusters including those with mixed-metals (such as $TiVO_5$ and $CrVO_6$) may have high oxidative reactivity that has not been experimentally identified. The chemical structures of radical oxygen over V_2O_5/SiO_2 and MoO_3/SiO_2 catalysts are suggested and the balance between high reactivity and low concentration of the radical oxygen in condensed phase catalysis is discussed.

Keywords DFT · Transition metal oxide clusters · Bonding property · Oxygen-centered radical

1 Introduction

Transition metal oxides (TMOs) are widely used as both catalysts [1–3] and catalyst-support materials [4–7] for numerous commercially relevant reactions, for example, the selective oxidation of SO_2 to SO_3 in the production of sulfuric acid [8], the selective reduction in nitrogen oxides by NH_3 [9], the oxidation of carbon monoxide to eliminate harmful environmental substance [10], and the partial oxidation of volatile organic compounds to produce valuable chemicals [11–13]. Numerous investigations were carried out to understand the mechanisms of catalytic oxidations over TMO surfaces. It was suggested that the O^- radical (or $O^{\cdot}$) is the most important species in several selective oxidation reactions [14, 15]. It was usually considered that the O^- radical species is unstable on TMO surface. However, some experiments evidenced that the O^- species can be stable on supported vanadium and molybdenum oxides even at 300 °C [16, 17]. The electron paramagnetic resonance spectroscopy study of partial oxidation of methane to methanol and formaldehyde by nitrous oxide over silica-supported molybdenum oxides supported a mechanism that the reaction is initiated by the formation of O^- radical coordinated with Mo (VI) at the surface [16–19]. Similar mechanism of methane partial oxidation was also proposed over silica-supported vanadium pentoxide in the temperature range of 460–500 °C

Electronic supplementary material The online version of this article (doi:10.1007/s00214-010-0732-8) contains supplementary material, which is available to authorized users.

Y.-X. Zhao · X.-L. Ding · Y.-P. Ma · Z.-C. Wang · S.-G. He (✉)
Beijing National Laboratory for Molecular Science, State Key Laboratory for Structural Chemistry of Unstable and Stable Species, Institute of Chemistry, Chinese Academy of Sciences, 100190 Beijing, People's Republic of China
e-mail: shengguihe@iccas.ac.cn

Y.-X. Zhao · Z.-C. Wang
Graduate School of Chinese Academy of Sciences, 100039 Beijing, People's Republic of China

[20]. The O^- radical was also suggested to be active form of oxygen in the oxidative dehydrogenation of ethane over partially reduced MoO_3 supported on silica [21]. The study of methane conversion to formaldehyde over monomeric vanadium oxide supported on mesoporous silica suggested that (V^{4+}–O^-) species which was detected by Raman spectroscopy is reactive intermediate, and it was proposed that the O^- species is formed by proton migration from the VOH group to the support [22]. Recently, the oxidation of benzene by N_2O to phenol with 100% selectivity over iron-containing zeolites (ZSM-5, MFI, and Beta) provided reliable evidence that the radical O^- is involved in the overall catalytic process [23–26].

Due to difficulty in the characterizations of surface chemical structures, the roles of the radical oxygen $O^{\cdot}$ in TMO catalysis remain poorly understood in details. Isolated gas phase TMO clusters ($M_xO_y^q$, in which M is the metal atom and q is the charge number) are actively studied as model systems to obtain molecular-level information for condensed phase catalytic processes [27–36]. The cluster systems enable the investigation into catalysis in the absence of factors which may complicate condensed phase studies. Fruitful results were yielded in the studies of isolated TMO clusters using both experiments and theoretical calculations [37–61]. The experimental investigations into $M_xO_y^q$ reactivity toward small molecules such as hydrocarbons (CH_4, $C_2H_{2,4,6}$, etc.) and carbon monoxide (CO) identified that only clusters with specific compositions are highly oxidative. These oxidative TMO clusters including neutrals, cations, and anions usually contain the oxygen-centered radical ($O^{\cdot}$).

For neutral TMO clusters, only VO_3, V_3O_8, and V_5O_{13} [$VO_3(V_2O_5)_{0-2}$] clusters are experimentally reported to contain the $O^{\cdot}$ [37–39]. The reactions of $VO_3(V_2O_5)_{0-2}$ toward alkenes are followed by C=C double bond cleavage under near room temperature conditions. These clusters can also oxidize benzene molecules to produce water [39]. In contrast to the much less studied neutral TMO cluster systems, many cationic and some anionic TMO clusters with oxygen-centered radical were reported in literature.

Reactions of $V_2O_5^+$, $V_4O_{10}^+$, and $V_6O_{15}^+$ [$(V_2O_5)_{n=1-3}^+$] clusters with C_2H_4 produce CH_3CHO via radical-cation mechanism [40–43]. The $V_4O_{10}^+$ cluster with the unpaired electron being localized at one of the four terminal vanadyl oxygen atoms has the ability to activate alkanes and alkenes including CH_4, C_2H_6, C_3H_8, C_4H_{10}, C_3H_6 and C_4H_8 [44–46]. $V_4O_{10}^+$ cluster is also the first and so far only example of polynuclear TMO clusters for activation of CH_4 under thermal collision condition [45]. $Nb_2O_5^+$ and $Ta_2O_5^+$ clusters also possess radical oxygen, but the experiments indicated that they are less reactive than $V_2O_5^+$ in reactions with C_4H_{10} and C_4H_6 [47]. Radical-cations MoO_3^+ [48] and OsO_n^+ ($n = 1, 2, 4$) [49] can activate C–H bond of CH_4. In addition, it was also reported that $(MoO_3)_{1-3}^+$ clusters are oxidative toward CO and c-C_3H_6 through oxygen atom transfer and dehydrogenation reactions, respectively [50]. Recent experiments suggested that cationic $(WO_3)_{1-3}^+$ clusters can transfer a single oxygen atom to C_3H_6 and CO due to the presence of radical oxygen in these clusters [51]. It has been demonstrated that TiO_2^+ cluster is able not only to activate alkanes but also to seize a hydrogen atom from water molecule due to the radical oxygen character [52]. Recent experimental and theoretical studies [53] concluded that all of the $(ZrO_2)_{1-4}^+$ clusters possess oxygen-centered radical and it is facile to transfer a single oxygen atom from these clusters to CO, C_2H_2, and C_2H_4 molecules; moreover, hydrogen atom abstraction from C_2H_4 by $(ZrO_2)_{1-4}^+$ was also suggested [54]. Besides TMO clusters, some main-group metal oxide cluster cations also have the character of oxygen-centered radical. MgO^+ [55] and $(Al_2O_3)_{3-5}^+$ [56, 57] clusters with the spin density being almost exclusively located at a single oxygen atom have the ability to activate CH_4 at room temperature.

The $V_2O_6^-$ and $V_4O_{11}^-$ clusters are oxidative toward butene and 1,3-butadiene through loss of a single oxygen atom [58]. High efficiency of the oxygen transfer can occur in the reaction of propene with $V_4O_{11}^-$ cluster to produce C_3H_6O and C_3H_4O under the condition of photon initiation [59]. Experimental and theoretical studies also concluded that $Zr_nO_{2n+1}^-$ ($n = 1$–4) clusters possess oxygen-centered radical although they are less oxidative than $(ZrO_2)_{1-4}^+$ in the reactions with CO, C_2H_2, and C_2H_4 due to the different molecular electrostatic potentials for the clusters in different charge states [60, 61].

The aforementioned statements indicate that the TMO clusters with oxygen-centered radical were only reported case by case. Systematic study may be required to clarify what type of TMO clusters have oxygen-centered radical and how the bonding and reactivity of these clusters depend on the metal type, cluster size, charge state, and so on. A careful analysis of the relationship of valence state, atomic number, and charge state of the radical oxygen containing TMO clusters reported in literature and mentioned above, we suggest that early transition metal oxide clusters $M_xO_y^q$ with $\Delta \equiv 2y - nx + q = 1$, in which n is the number of metal valence electrons and q is the charge number, may all have the character of oxygen-centered radical. This study is to clarify the above statement by a DFT study of the group 3 (Sc, Y, La), group 4 (Ti, Zr, Hf), group 5 (V, Nb, Ta), group 6 (Cr, Mo, W), and group 7 (Mn, Tc, Re) TMO clusters with limited number of metal atoms. We hope that our results can contribute to the comprehension of the importance of radical oxygen in condensed phase catalysis.

It should be pointed out that for positively charged systems ($q = +1$), the $\Delta = 1$ clusters are stoichiometric

transition metal oxide species such as $(Sc_2O_3)_k^+$, $(TiO_2)_k^+$, $(V_2O_5)_k^+$, $(CrO_3)_k^+$, and $(Mn_2O_7)_k^+$ which may be generated by exciting one electron from the stoichiometric neutral clusters into vacuum. The unpaired electron left in the cations can be localized on the oxygen atom(s) to form oxygen-centered radical under the condition that all of the metal atoms are in the maximum oxidation state (MOS). For bulk materials such as TiO_2 and V_2O_5, such condition (metal in MOS) can be satisfied for the lattice metal atoms but may not be satisfied for surface metal atoms, especially those involved with steps and defects. It is thus not obvious the condition of metal in MOS can be satisfied for transition metal oxide cluster systems in the gas phase because it is generally considered that atoms in small clusters are surface-character. Meanwhile, it has been demonstrated by both experiments and theoretical calculations that the charge states may influence the geometrical and electronic structures of a cluster significantly. For example, an O_2 moiety can be end-on, side-on, and inserted bonded in the ground state structures of $Fe_2O_5^+$, Fe_2O_5, and $Fe_2O_5^-$, respectively [62]. As a result, it is very necessary to study whether all of the $\Delta = 1$ clusters including cations, anions, and neutrals have the character of oxygen-centered radical although from the literature studies one may consider that all of the stoichiometric transition metal oxide cations ($\Delta = 1$) belong to this type.

2 Computational details

The theoretical calculations are carried out by using the Gaussian 03 program [63]. Geometry optimizations and frequency calculations are performed with the hybrid B3LYP exchange–correlation functional [64–66]. All-electron polarized triple-ζ valence basis sets (TZVP) [67] are used for O and 3d transition metal atoms (Sc–Mn), and the effective core potentials (ECPs) [68] and the polarized triple-ζ valence basis sets (Def2-TZVP) [68, 69] are used for 4d (Y–Tc) and 5d (La–Re) transition metal atoms. Benchmark calculations of the bond distances, bond dissociation, ionization, and electron affinity energies are performed for all of the transition metal monoxides with B3LYP method. The studied $M_xO_y^q$ clusters with $\Delta = 1$ (see Introduction section for the definition of Δ) are listed in Table 1. All of the clusters containing up to three metal atoms are included. Results of larger clusters (up to six metal atoms) are only obtained for $Sc_xO_y^q$ clusters. To predict the oxygen dissociation energy of $M_{x\leq 3}O_y^q$ clusters, the geometries of $M_{x\leq 3}O_{y-1}^q$ ($\Delta = -1$) clusters are also optimized at the B3LYP level.

In order to obtain the lowest energy structure for each cluster at the adopted level of theory, the geometry optimizations were performed starting from as many different geometry types as possible. All possible spin multiplicities for each geometry are also tested to find the most stable electronic state. All structures presented in this paper are fully optimized and vibrational frequency analysis is performed to ensure that the optimized geometries are minima. Zero-point vibrational energy correction is taken into account throughout this work. The structures of $M_xO_y^q$ clusters containing one to three metal atoms ($x = 1$–3) are relatively simple and it is possible to get the global minima based on chemical intuitions. It is our conjecture that the global minimum structures for these $M_xO_y^q$ clusters with $x = 1$–3 have been obtained. For larger clusters ($Sc_xO_y^q$, $x \geq 4$), although many structure types have been tested and the relative stable structures are determined under the adopted computational level, special global optimization techniques such as genetic algorithms [57] may be necessary to find the true global minima. In addition, the Wiberg bond orders are calculated for MO_y^q clusters using the NBO 3.1 program [70] that is implemented in the Gaussian 03 software package.

It was demonstrated by Dixon and coauthors that, due to the presence of substantial Hartree–Fock (HF) exchange component, the hybrid B3LYP functional often leads to

Table 1 The studied $M_xO_y^q$ clusters with $\Delta = 1$

Group	3		4		5		6		7	
MO_y^q	ScO_2		TiO_2^+	TiO_3^-	VO_3		CrO_3^+	CrO_4^-	MnO_4	
	YO_2		ZrO_2^+	ZrO_3^-	NbO_3		MoO_3^+	MoO_4^-	TcO_4	
	LaO_2		HfO_2^+	HfO_3^-	TaO_3		WO_3^+	WO_4^-	ReO_4	
$M_2O_y^q$	$Sc_2O_3^+$	Sc_2O_4-	$Ti_2O_4^+$	$Ti_2O_5^-$	$V_2O_5^+$	$V_2O_6^-$	$Cr_2O_6^+$	$Cr_2O_7^-$	$Mn_2O_7^+$	$Mn_2O_8^-$
	$Y_2O_3^+$	Y_2O_4-	$Zr_2O_4^+$	$Zr_2O_5^-$	$Nb_2O_5^+$	$Nb_2O_6^-$	$Mo_2O_6^+$	$Mo_2O_7^-$	$Tc_2O_7^+$	$Tc_2O_8^-$
	$La_2O_3^+$	La_2O_4-	$Hf_2O_4^+$	$Hf_2O_5^-$	$Ta_2O_5^+$	$Ta_2O_6^-$	$W_2O_6^+$	$W_2O_7^-$	$Re_2O_7^+$	$Re_2O_8^-$
$M_3O_y^q$	Sc_3O_5		$Ti_3O_6^+$	$Ti_3O_7^-$	V_3O_8		$Cr_3O_9^+$	$Cr_3O_{10}^-$	Mn_3O_{11}	
	Y_3O_5		$Zr_3O_6^+$	$Zr_3O_7^-$	Nb_3O_8		$Mo_3O_9^+$	$Mo_3O_{10}^-$	Tc_3O_{11}	
	La_3O_5		$Hf_3O_6^+$	$Hf_3O_7^-$	Ta_3O_8		$W_3O_9^+$	$W_3O_{10}^-$	Re_3O_{11}	
$M_{4-6}O_y^q$	$Sc_4O_6^+$, $Sc_4O_7^-$, Sc_5O_8, $Sc_6O_9^+$, $Sc_6O_{10}^-$									

symmetry breaking structures (lower-symmetry structures) for early transition metal oxide clusters, especially the 3d metal oxide species [71–76]. In contrast, the pure generalized gradient approximation (GGA) functional such as BPW91 [64, 77] usually leads to high-symmetry structures. For comparison, the BPW91 functional and the same basis sets used in the B3LYP calculations are also employed to optimize geometries for most of the $M_xO_y^q$ clusters with $x = 1$ and 2 and some of them with $x = 3$. In the case that the B3LYP and BPW91 predict very different ground state structures, single-point energy calculation at the U/UCCSD(T) [78, 79] level is performed to decide what result is more reliable. The T_1 diagnostics [80] for the ground state of CrO_3^+ from U/UCCSD(T) calculation are also performed.

3 Results

3.1 B3LYP method on transition metal monoxides

Benchmark calculations of bond distances (R_e), bond dissociation energies (D_0), adiabatic ionization (IE_{ad}), and electron affinity (EA_{ad}) energies are performed for the 3d, 4d, and 5d transition metal monoxides at B3LYP level. The calculated and available experimental results are summarized in Table 2. The computed R_e values of the 3d, 4d, and 5d monoxides agree with the experimental results within −0.011–0.016 Å. The deviations of computed D_0, IE_{ad}, and EA_{ad} of the 3d metal species from the experimental values are relatively small. With exception of the D_0 value of CrO, which is underestimated by 0.63 eV at the B3LYP level, the deviations of the calculations from the experiments are within −0.07 to −0.24 eV, −0.06 to +0.18 eV, and −0.28 to −0.41 eV for the D_0, IE_{ad}, and EA_{ad} values of the 3d metal monoxides, respectively. The deviations of the computed D_0, IE_{ad}, and EA_{ad} of 4d metal monoxides from the experimental values are also not very large, and they are within 0.00 to −0.33 eV, +0.14 to +0.63 eV, and −0.08 to −0.21 eV, respectively. For 5d transition metal monoxides, most of the D_0, IE_{ad}, and EA_{ad} values can be predicted with accuracy being similar to the 3d and 4d systems. The worst predictions are on the D_0 values of LaO and ReO which are underestimated by −1.04 and −1.60 eV, respectively. With the possibility that the above two large deviations may be partly due to the experimental uncertainties, we can still conclude that with only a few exceptions, the B3LYP functional and employed basis sets are able to predict the D_0, IE_{ad}, and EA_{ad} values of the early transition metal monoxides and O_2 molecule (see the last column of Table 2) with reasonably good accuracy.

3.2 Stoichiometry of $M_xO_y^q$ clusters with $\Delta = 1$

The TMO clusters $M_xO_y^q$ with $\Delta = 1$ are $(M_2O_3)_kMO_2$, $(M_2O_3)_k^+$, and $(M_2O_3)_kM_2O_4^-$ for group 3 metals (M = Sc, Y, La); $(MO_2)_k^+$ and $(MO_2)_kMO_3^-$ for group 4 (M = Ti, Zr, Hf); $(M_2O_5)_kMO_3$, $(M_2O_5)_k^+$, and $(M_2O_5)_kM_2O_6^-$ for group 5 (M = V, Nb, Ta); $(MO_3)_k^+$ and $(MO_3)_kMO_4^-$ for group 6 (M = Cr, Mo, W); and $(M_2O_7)_kMO_4$, $(M_2O_7)_k^+$, and $(M_2O_7)_kM_2O_8^-$ for group 7 (M = Mn, Tc, Re). The specific clusters containing up to three metal atoms are listed in Table 1. The neutral M_xO_y clusters that can satisfy $\Delta = 1$ are only groups 3, 5, and 7 metal species. Cluster cations and anions $M_xO_y^\pm$ with $\Delta = 1$ can be any group of the transition metal species.

3.3 Structure and bonding

3.3.1 Clusters with one metal atom

The most stable structures of MO_y^q ($\Delta = 1$) clusters by B3LYP are displayed in Fig. 1. Each of the dioxides MO_2 (group 3) and MO_2^+ (group 4) has two separate metal–oxygen terminal bonds. In this study, the terminal oxygen atom and terminal M–O bond are denoted as O_t and M–O_t, respectively. The point group symmetries of these clusters are either C_s (ScO_2, TiO_2^+, ZrO_2^+) or C_{2v} (YO_2, LaO_2, HfO_2^+). For the C_s symmetry clusters, one of the M–O_t bond lengths (1.91, 1.68, and 1.81 Å for Sc–O, Ti–O, and Zr–O, respectively) is significantly longer than the other (1.70, 1.64, and 1.77 Å). YO_2, LaO_2, and HfO_2^+ clusters have the same electronic ground state, $^2B_2$. The M–O_t bonds of YO_2 (1.92 Å), LaO_2 (2.05 Å), and HfO_2^+ (1.80 Å) are significantly longer than those of the diatomic molecules YO (1.81 Å), LaO (1.93 Å), and HfO (1.74 Å) at the B3LYP level.

With only exception of CrO_3^+, each of the trioxides MO_3^- (group 4), MO_3 (group 5), and MO_3^+ (group 6) has three separate M–O_t bonds. The clusters are either C_s or C_{2v} symmetry. One of the M–O_t bonds of each of the MO_3^q clusters (except CrO_3^+) is longer than the other two by 0.13–0.21 Å. The bonding property of CrO_3^+ cluster shown in Fig. 1 is apparently different from those of the other trioxides. There is a side-on bonded (η^2–) O_2 unit with O–O length of 1.30 Å in CrO_3^+. The distance between Cr and the η^2–O_2 is quite long (Cr–O = 1.91 Å) while the length of the Cr–O_t bond is short (1.54 Å). The structures and relative energies of two CrO_3^+ isomers with and without η^2–O_2 by B3LYP and BPW91 are given in Fig. 2a. The B3LYP predicts that CrO_3^+ with η^2–O_2 is the ground state while the BPW91 predicts that the isomer with three Cr–O_t bonds is the ground state.

The relative U/UCCSD(T) single-point energies of CrO_3^+ at the B3LYP optimized ground state ($C_s/^2A'$, with

Table 2 Bond distances (R_e, in Å), dissociation (D_0), adiabatic ionization (IE_{ad}), and electron affinity (EA_{ad}) energies (in eV) of *M*O and O_2 molecules by B3LYP and experiments

	3d					4d					5d					
	^{2}ScO	^{3}TiO	^{4}VO	^{5}CrO	^{6}MnO	^{2}YO	^{1}ZrO	^{4}NbO	^{5}MoO	^{6}TcO	^{2}LaO	^{1}HfO	^{2}TaO	^{3}WO	^{4}ReO	$^3O_2$
R_e																
Calc.	1.669	1.621	1.590	1.624	1.638	1.806	1.720	1.690	1.700	1.729	1.929	1.736	1.696	1.663	1.691	1.208
Expt.	1.66826[a]	1.62022[a]	1.58932[a]	1.615[a]	1.646[b]	1.790[a]	1.7116[a]	1.6909[a]	1.70[b]	No	No	1.723071[a]	1.68746[a]	1.666[b]	1.702[b]	1.20752[a]
D_0																
Calc.	6.70	6.67	6.30	4.15	3.76	7.01	7.66	7.53	5.30	5.41	7.15	8.09	7.75	6.98	4.86	5.11
Expt.	6.94[c] ± 0.09	6.87[c] ± 0.07	6.44[c] ± 0.2	4.78[c] ± 0.09	3.83[c] ± 0.08	7.337[d]	7.94[e] ± 0.11	7.53[e] ± 0.11	5.44[e] ± 0.04	5.64[f] ± 0.87	8.19[g] ± 0.04	8.19[g] ± 0.09	8.30[g] ± 0.13	7.01[h] ± 0.31	6.46[f] ± 0.87	5.116[f] ± 0.002
IE_{ad}																
Calc.	6.53	6.99	7.42	8.18	8.64	6.35	7.44	7.42	7.59	8.68	5.59	7.83	7.93	7.96	8.49	12.63
Expt.	6.562[i]	6.8197[e] ± 0.007	7.2386[i] ± 0.0004	8.16[i] ± 0.01	8.65[i] ± 0.2	5.85[i] ± 0.15	6.812[e] ± 0.002	7.154[e] ± 0.001	7.4504[e] ± 0.0005	No	4.9[i]	7.91687[i] ± 0.0001	8.61[i] ± 0.02	8.04[h] ± 0.45	No	12.07[i] ± 0.000248
EA_{ad}																
Calc.	1.07	0.96	0.82	0.88	1.02	1.27	1.13	1.08	1.19	1.30	1.04	0.44	0.95	0.81	1.62	0.32
Expt.	1.35[c] ± 0.02	1.30[c] ± 0.03	1.229[c] ± 0.008	1.221[c] ± 0.006	1.375[c] ± 0.01	1.35[j] ± 0.02	1.3[j] ± 0.3	1.29[j] ± 0.02	1.290[j] ± 0.006	No	No	No	1.07[j] ± 0.06	No	No	0.448[j] ± 0.006

[a] Ref. [81]

[b] Refs. [82–84]. Ref. [82]: MnO, Ref. [83]: MoO, Ref. [84]: WO and ReO

[c] Ref. [85]

[d] Ref. [86]

[e] Ref. [87]

[f] Ref. [88]

[g] Refs. [89–91]. Ref. [89]: LaO, Ref. [90]: HfO, Ref. [91]: TaO

[h] Ref. [92]

[i] Refs. [93–101]. Ref. [93]: ScO, Ref. [94]: VO, Ref. [95]: CrO, Ref. [96]: MnO, Ref. [97]: YO, Ref. [98]: LaO, Ref. [99]: HfO, Ref. [100]: TaO, Ref. [101]: O_2

[j] Refs. [102–107]. Ref. [102]: YO, Ref. [103]: ZrO, Ref. [104]: NbO, Ref. [105]: MoO, Ref. [106]: TaO, Ref. [107]: O_2

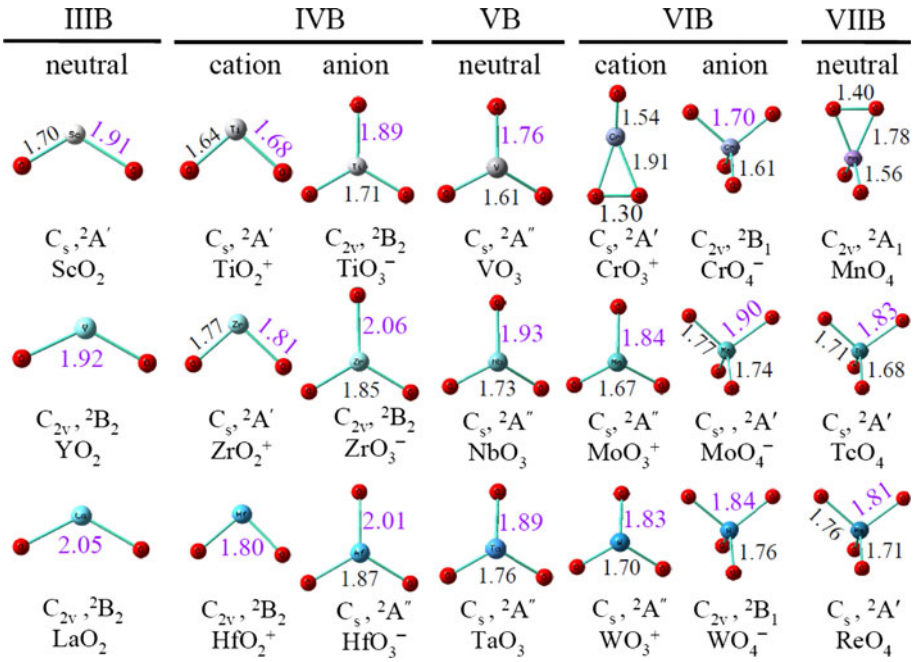

Fig. 1 B3LYP optimized structures of MO_y^q ($\Delta = 1$) clusters. The bond lengths in Å are given. Note that the electronic state of WO_4^- may be labeled as $^2B_2$ if the labeling of the two symmetry planes (σ_{xz} and σ_{yz}) of the C_{2v} point group switches

η^2–O_2 unit) and the BPW91 ground state ($C_{3v}/^2A_2$, without η^2–O_2 unit) are 0.0 and 0.27 eV, respectively. The T_1 diagnostic value for the $^2A'$ state of CrO_3^+ [B3LYP/Fig. 2a (1)] from the U/UCCSD(T) calculations is about 0.083 when frozen-core approximation is applied and 0.059 otherwise, while for $^2A_2$ state of CrO_3^+ [BPW91/Fig. 2a (2)] the T_1 diagnostic value ranges from 0.119 to 0.168. The large T_1 diagnostic values reveal that methods based on single-reference wave-functions are insufficient for accurate modeling of CrO_3^+ system, and those based on multi-reference wave-functions such as CASSCF and MRCI may be more appropriate.

With only exception of MnO_4, each of the tetra-oxides MO_4^- (group 6) and MO_4 (group 7) has four separate M–O_t bonds. The clusters are either C_s or C_{2v} symmetry. Similar as trioxides, one or two of the M–O_t bonds of each of the MO_4^q cluster (except MnO_4) are significantly longer than the other three or two. Comparison of the results of two MnO_4 isomers with and without η^2–O_2 moiety at different levels is given in Fig. 2b. Similar as in CrO_3^+, it is more

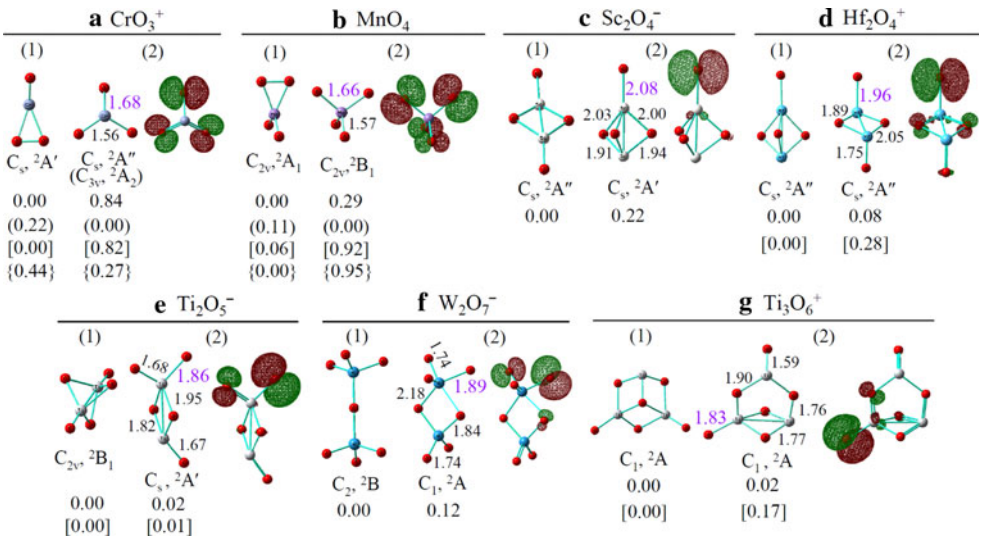

Fig. 2 B3LYP optimized structures and relative energies (in eV) of two isomers of CrO_3^+ (**a**), MnO_4 (**b**), $Sc_2O_4^-$ (**c**), $Hf_2O_4^+$ (**d**), $Ti_2O_5^-$ (**e**), $W_2O_7^-$ (**f**), and $Ti_3O_6^+$ (**g**). The relative energies of CrO_3^+ and MnO_4 optimized by BPW91 are given in the *parentheses*. The isomer (2) of CrO_3^+ has C_{3v} symmetry by BPW91. The U/UCCSD(T) single-point energies at the B3LYP optimized isomeric structures are given in the *square brackets*. For CrO_3^+ and MnO_4, the U/UCCSD(T) single-point energies at the BPW91 optimized isomeric structures are given in the *braces*. The bond lengths in Å are given. The SOMO of higher energy isomer is also shown for each cluster

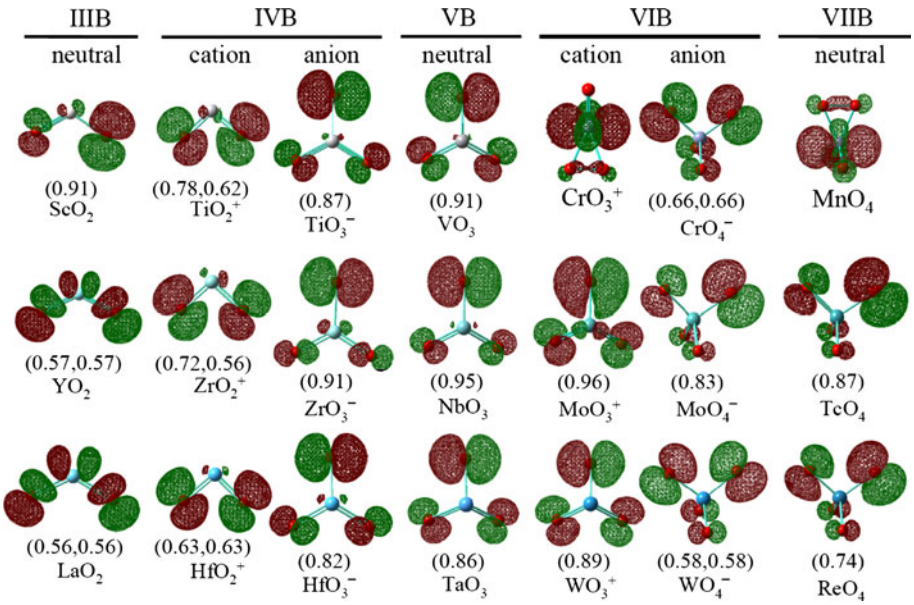

Fig. 3 The SOMOs of MO_y^q ($\Delta = 1$) clusters. The orientation of each cluster is the same as the one in Fig. 1. The Mulliken spin density values (greater than 0.5 μ_B) over oxygen atoms are given in the *parentheses*

reliable to conclude that the MnO_4 isomer with η^2–O_2 is the ground state.

All of the clusters shown in Fig. 1 have doublet spin multiplicity and each of them has one unpaired electron. To further understand the bonding properties, Figs. 3 and 1SI plot the profiles of singly occupied molecular orbitals (SOMOs, the MOs are the Kohn–Sham orbitals by DFT) and the electron spin density distribution, respectively. The Mulliken spin density values (greater than 0.5 μ_B) over oxygen atoms are also given in Fig. 3. The profiles of SOMOs and spin density for MO_y^q are similar. With two exceptions of CrO_3^+ and MnO_4, the SOMOs of all of the clusters are with character of oxygen 2p orbitals. The spin density (or unpaired electron) is mainly localized over a single terminal oxygen atom in ScO_2, MO_3^- (group 4), MO_3 (group 5), MoO_3^+, WO_3^+, MoO_4^-, TcO_4, and ReO_4 clusters and it is mainly localized over two terminal oxygen atoms in all of the other clusters. The O_t atoms with high (>0.5 μ_B) spin density are denoted as $O_t^{\cdot}$ in this study.

Figure 2SI plots the optimized structures of one-oxygen-less clusters MO_{y-1}^q ($\Delta = -1$) for those MO_y^q ($\Delta = 1$) in Fig. 1. Wiberg bond order analysis shows that the bond orders for M–O_t bonds in MO^+ (M = Ti, Zr, Hf), MO_2 (M = V, Nb, Ta), and MO_2^+ (M = Mo, W) clusters are close to 2.0, which means that the M–O_t bonds in these $\Delta = -1$ clusters are typical $M = O$ double bonds. The M–O_t bond orders for all of the other clusters in Fig. 2SI are in the range of 1.46–1.79, indicating these M–O_t bonds are in between typical single and double bonds. Comparison of the bond lengths indicates that all of the M–$O_t^{\cdot}$ bonds (Figs. 1, 3) are longer than the corresponding M–O_t bonds (Fig. 2SI) by as large as 0.25 Å (ZrO_3^- vs. ZrO_2^-) or at least 0.07 Å (CrO_4^- and WO_4^- vs. CrO_3^- and WO_3^-). For the clusters CrO_4^- and WO_4^- (C_{2v} symmetry) in the latter case, the unpaired electron is equally distributed over two $O_t^{\cdot}$ atoms, so the "net" bond length increase in a single M–$O_t^{\cdot}$ over normal M–O_t may be estimated as 2×0.07 Å = 0.14 Å, which is also very significant. The M–$O_t^{\cdot}$ bond orders are also computed. The values are close to or less than 1.0, for example, the bond order values are 1.14, 1.06, 0.80, 0.75 for Ta–$O_t^{\cdot}$ in TaO_3, Mo–$O_t^{\cdot}$ in MoO_4^-, Sc–$O_t^{\cdot}$ in ScO_2, and Zr–$O_t^{\cdot}$ in ZrO_3^-, respectively. These M–$O_t^{\cdot}$ bonds can be considered as M–O single bonds. From the unpaired electron distribution (Fig. 3) and the above bond length considerations, we propose that each of the clusters in Fig. 1 (except CrO_3^+ and MnO_4) contains one (or equivalently one, two halves) oxygen-centered radical that can be denoted as $O^{\cdot}$ or O^-.

3.3.2 *Clusters with two metal atoms*

The most stable structures of $M_2O_y^q$ ($\Delta = 1$) and $M_2O_{y-1}^q$ ($\Delta = -1$) clusters by B3LYP are displayed in Figs. 4 and 3SI, respectively. The SOMOs of $M_2O_y^q$ ($\Delta = 1$) are given in Fig. 5. A quick overview of the results indicates that although the structures of $M_2O_y^q$ ($\Delta = 1$) are generally very different from those of the MO_y^q ($\Delta = 1$), most of the di-metal oxides (exceptions are $Cr_2O_6^+$, $Cr_2O_7^-$, $Mn_2O_7^+$, and $Mn_2O_8^-$) contain the radical oxygen $O^{\cdot}$ with essentially the same characters (spin density distribution over oxygen 2p orbitals, lengthening of the M–$O^{\cdot}$ bonds compared with the normal M–O) as those of the $O^{\cdot}$ in the mono-metal oxides (Sect. 3.3.1).

The $M_2O_3^+$ (M = Sc, Y, La) clusters in Fig. 4 do not have any M–O_t bond. The unpaired electron in each of the $M_2O_3^+$ is thus located in two bridging oxygen (O_b) atoms and the radical oxygen (Fig. 5) in this case is denoted as $O_b^{\cdot}$. The electronic ground states for $Sc_2O_3^+$, $Y_2O_3^+$, and

$La_2O_3^+$ are all $^2B_2$ state (the plane containing three oxygen atoms is defined as σ_{yz}).

There are two types of structure isomers for $M_2O_4^-$ (group 3) and $M_2O_4^+$ (group 4): (1) two M–O_t bonds connecting with a four-membered ring (M–O_b–M–O_b) structure (ground state of $Sc_2O_4^-$, $Ti_2O_4^+$, and $Zr_2O_4^+$ by B3LYP), and (2) a single M–O_t bond connecting with a di-pyramid capped [M–$(O_b)_3$–M] structure ($Y_2O_4^-$, $La_2O_4^-$, and $Hf_2O_4^+$). Figure 2c–d shows that for $Sc_2O_4^-$ and $Hf_2O_4^+$, the two isomers are close in energy. The ground electronic states of $Sc_2O_4^-$, $Y_2O_4^-$, and $La_2O_4^-$ by B3LYP are $^2A''$, $^2A'$, and $^2A_1$, respectively. Test calculations indicate that $^2A'$ state of $Sc_2O_4^-$ is above the ground state $^2A''$ by 0.20 eV. It is interesting to note that in Fig. 5, the SOMO of $La_2O_4^-$ (mainly oxygen $2p_z$) is quite different from that of $Y_2O_4^-$ (mainly oxygen $2p_x$ or $2p_y$) due to higher symmetry of the former (C_{3v}) over the latter (C_s) (see Fig. 4).

Most of the $M_2O_5^{\pm}$ clusters have one M–O_b–M–O_b ring moiety and three M–O_t bonds. The only exception is $Ti_2O_5^-$ for which the isomer with three Ti–O_t bonds is slightly higher in energy than the one with two Ti–O_t bonds at the B3LYP level (Fig. 2e). It is interesting to note that in the predicted ground state of $Ti_2O_5^-$ (Figs. 4, 5), the unpaired electron is mainly located over two O_b atoms rather than the O_t atom(s).

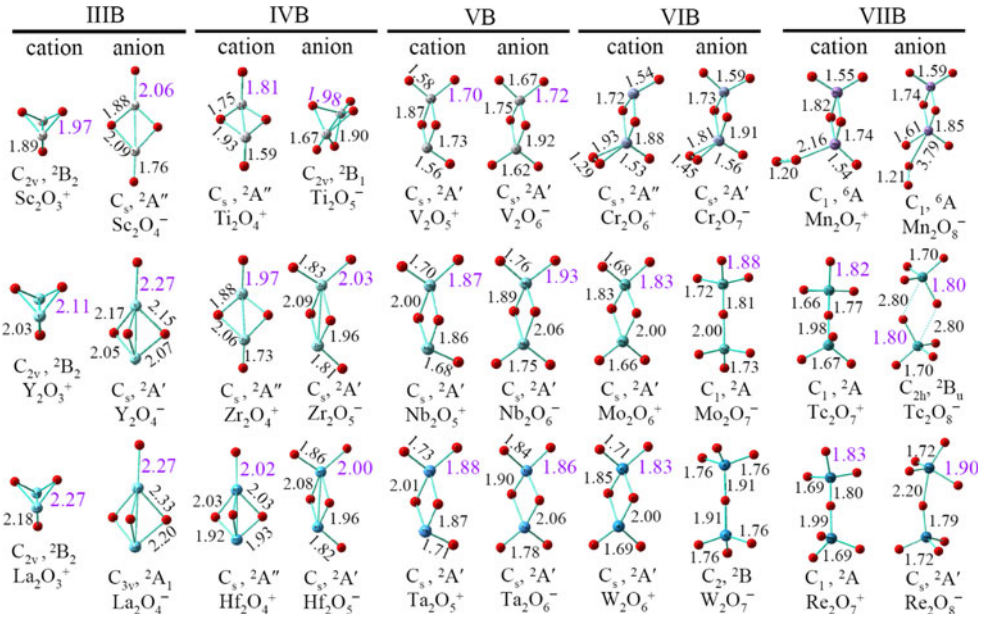

Fig. 4 B3LYP optimized structures of $M_2O_y^q$ ($\Delta = 1$) clusters. The bond lengths in Å are given

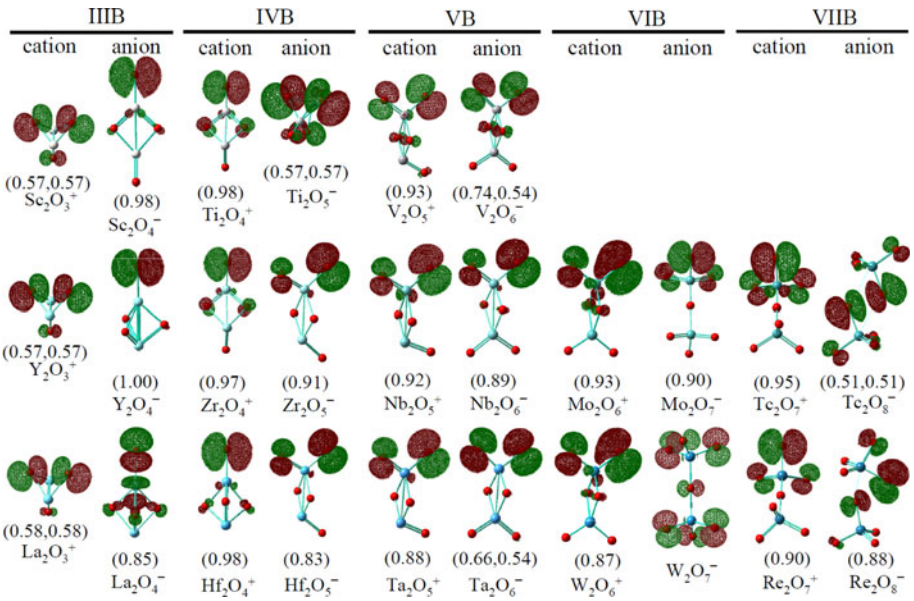

Fig. 5 The SOMOs of $M_2O_y^q$ ($\Delta = 1$) clusters. The orientation of each cluster is the same as the one in Fig. 4. The Mulliken spin density values (greater than 0.5 μ_B) over oxygen atoms are given in the *parentheses*

Except for $Cr_2O_6^+$ which has a η^2–O_2 moiety, each of the $M_2O_6^{\pm}$ clusters has one M–O_b–M–O_b ring moiety and four M–O_t bonds. $Cr_2O_7^-$ and $Mn_2O_7^+$ contain a η^2–O_2 and a η^1–O_2 (end-on bonded O_2), respectively. Structures of $Mo_2O_7^-$, $W_2O_7^-$, $Tc_2O_7^+$, and $Re_2O_7^+$ can be considered as two MO_3 units connected by one additional O_b atom. For $W_2O_7^-$, the two structural isomers with six and five W–O_t bonds are very close in energy and the unpaired electron is mainly localized over one O_t atom in the latter cluster (Fig. 2f) and almost equally distributed over six O_t atoms in the former one (Fig. 5). There is a η^1–O_2 unit in $Mn_2O_8^-$ cluster. $Tc_2O_8^-$ contains two loosely bounded TcO_4 units, and the unpaired electron is equally shared by the two units (Figs. 4, 5). Structure of $Re_2O_8^-$ can be

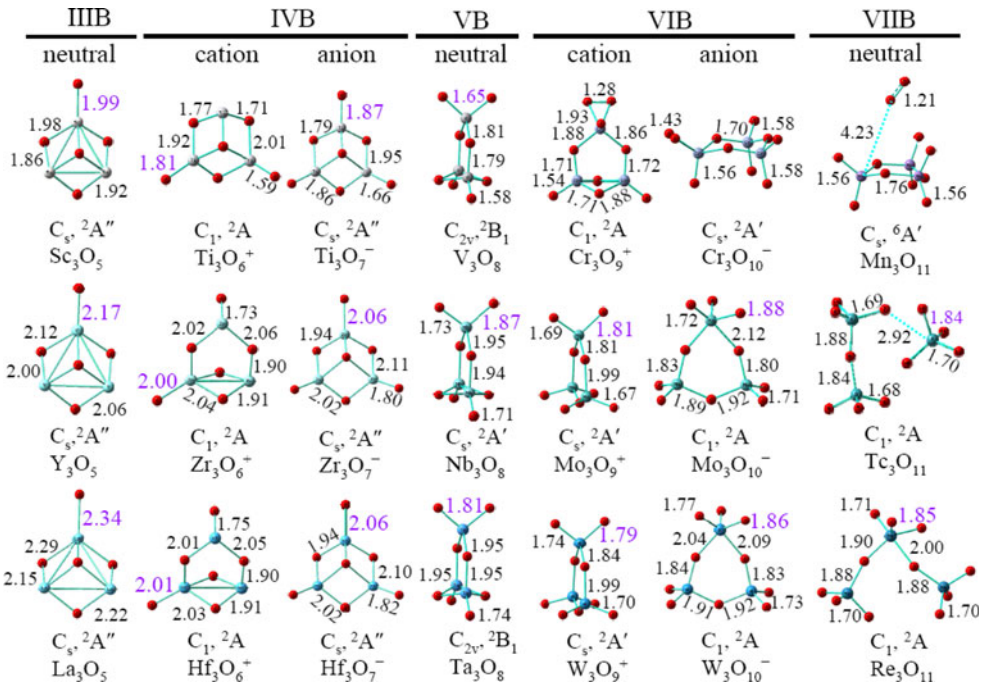

Fig. 6 B3LYP optimized structures of $M_3O_y^q$ ($\Delta = 1$) clusters. The bond lengths in Å are given

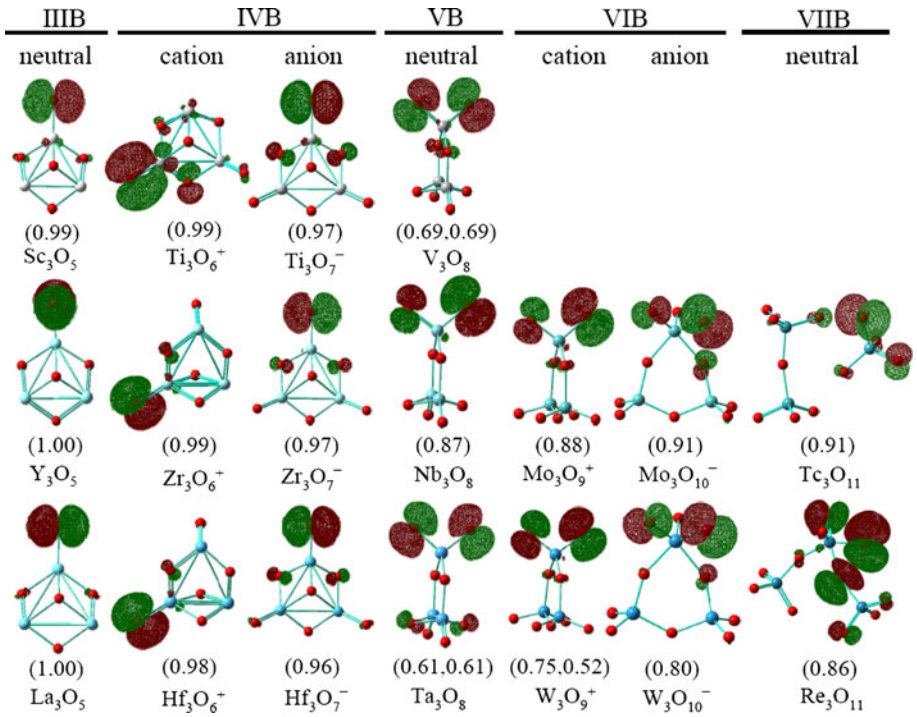

Fig. 7 The SOMOs of $M_3O_y^q$ ($\Delta = 1$) clusters. The orientation of each cluster is the same as the one in Fig. 6. The Mulliken spin density values (greater than 0.5 μ_B) over oxygen atoms are given in the *parentheses*

considered as ReO_3 and ReO_4 units connected by one additional O_b atom, and the unpaired electron is mostly located over one O_t atom in the ReO_4 unit.

3.3.3 Clusters with three metal atoms

The most stable structures of $M_3O_y^q$ ($\Delta = 1$) and $M_3O_{y-1}^q$ ($\Delta = -1$) clusters by B3LYP are displayed in Figs. 6 and 4SI, respectively. The SOMOs of $M_3O_y^q$ ($\Delta = 1$) are given in Fig. 7. Similar to the results of $M_2O_y^q$ ($\Delta = 1$) in Figs. 4 and 5 versus those of MO_y^q ($\Delta = 1$) in Figs. 1 and 3, the structures of $M_3O_y^q$ ($\Delta = 1$) are generally very different from those of the $M_{1,2}O_y^q$ ($\Delta = 1$), but most of the tri-metal oxides (exceptions are $Cr_3O_9^+$, $Cr_3O_{10}^-$, and Mn_3O_{11}) contain the radical oxygen $O^{\cdot}$ with essentially the same characters as those of the $O^{\cdot}$ in the mono-metal and di-metal oxides (Sects. 3.3.1, 3.3.2).

The structures of most of the $M_3O_y^q$ ($\Delta = 1$) clusters (except Cr and group 7 metal species) in Fig. 6 are all based on a six-membered ring structure (M–O_b–M–O_b–M–O_b) with appropriate number of additional O_t and O_b atoms. There is a special O_b atom which is threefold coordinated with metal atoms in the most stable structures of M_3O_5 (group 3), $Ti_3O_6^+$, and $M_3O_7^-$ (group 4). This kind of special O_b is denoted as O_b^{3f} and the notation O_b without a superscript denotes twofold coordinated bridging atom in the text below. Figure 2g shows that the structure isomer of $Ti_3O_6^+$ without the O_b^{3f} is slightly higher in energy than the one with the O_b^{3f}. Both $Cr_3O_9^+$ and $Cr_3O_{10}^-$ have a η^2–O_2. There is a O_2 unit far (4.23 Å) away from the nearest metal atom in Mn_3O_{11}. The structures of Tc_3O_{11} and Re_3O_{11} (Fig. 6) can be considered as those of $M_2O_7^-$ (Fig. 3SI, M = Tc and Re) and MO_4 (Fig. 1) weakly and relatively strongly bonded together, respectively. It is noticeable that one of the metal atoms in $Mo_3O_{10}^-$, $W_3O_{10}^-$, and Re_3O_{11} can be fivefold coordinated with two O_b and three O_t atoms.

3.3.4 Scandium oxide clusters with 4–6 metal atoms

The most stable structures and SOMOs of $Sc_{4-6}O_y^q$ ($\Delta = 1$) clusters by B3LYP are displayed in Fig. 8. Each of the Sc and O atoms of $Sc_4O_6^+$ and $Sc_6O_9^+$ is three and twofold coordinated, respectively, and the clusters are with cage structures. It is noticeable that the cage structures were also identified for transition metal oxide systems such as $(TiO_2)_n$ [108], $(V_2O_5)_n$ [109], $(CrO_3)_n$ [71, 73], and $(Fe_2O_3)_n$ [110]. The unpaired electron is mainly localized over a single O_b atom in $Sc_4O_6^+$ and $Sc_6O_9^+$ clusters. There is not a simple way to describe the structures of $Sc_4O_7^-$, Sc_5O_8, and $Sc_6O_{10}^-$. However, the radical oxygen $O_t^{\cdot}$ ($Sc_4O_7^-$ and Sc_5O_8,) or $O_b^{\cdot}$ ($Sc_6O_{10}^-$) still exists in these clusters. This implies that radical oxygen may also exist in larger sizes of other early transition metal oxide clusters $M_{x>3}O_y^q$ ($\Delta = 1$).

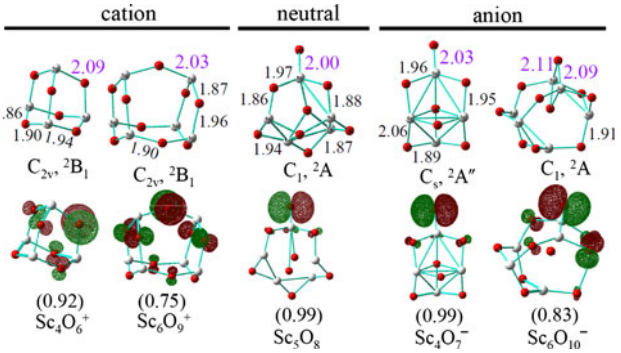

Fig. 8 B3LYP optimized structures and SOMOs of $Sc_{4-6}O_y^q$ ($\Delta = 1$) clusters. The bond lengths in Å are given. The Mulliken spin density values (greater than 0.5 μ_B) over oxygen atoms are given in the *parentheses*

3.4 Dissociation energies

Table 3 lists the energy costs of dissociation of one oxygen atom from the clusters (Figs. 1, 4, 6) with character of oxygen-centered radical. The listed dissociation energies (D_0) are calculated with $D_0(M_xO_y^q) = E(M_xO_{y-1}^q, \Delta = -1) + E(O, \text{triplet ground state})—E(M_xO_y^q, \Delta = 1)$, in which all of the energies (E) of the clusters are at the optimized structures (Figs. 1, 4, 6, 2SI–4SI) and with zero-point vibration corrections. Note that the IE of O atom (13.62 eV) is usually higher than those of the M_xO_{y-1} ($\Delta = -2$) clusters, for example, IE(HfO) $\approx$ 7.92 eV [99], IE(M_2O_4, M = V, Nb, Ta) < 10.5 eV [111], and IE(WO_2) = 12.5 eV [112]. In addition, the EA of O atom (1.46 eV) is usually smaller than those of the M_xO_y ($\Delta = 0$) clusters, such as TiO_2 (EA = 1.59 eV [113]) and CrO_3 (EA = 3.66 eV [73]). As a result, the alternative dissociation channels $M_xO_y^+ \rightarrow M_xO_{y-1} + O^+$ and $M_xO_y^- \rightarrow M_xO_{y-1} + O^-$ are expected to be subject to higher dissociation energies than those listed in Table 3, and these channels are not considered in this study. The D_0 values of $M_{1-3}O_y^q$ ($\Delta = 1$) by B3LYP in Table 3 cover a broad energy range from 1.90 eV (Tc_3O_{10}) to 5.06 eV ($Ta_2O_6^-$). The D_0 may be classified into three ranges: <3.0 eV (R-I), 3.0–4.0 eV (R-II), and >4.0 eV (R-III). More than half (37 of 63) of the D_0 values are in R-III. Only five of the D_0 (Tc_3O_{11}/1.90 eV, Re_3O_{11}/2.61 eV, $V_2O_5^+$/2.78 eV, $Mo_3O_{10}^-$/2.98 eV, $Tc_2O_8^-$/2.65 eV) are in R-I. The clusters with D_0 in R-II are either 3d metal (Sc, Ti, V) or group 6/7 metal (Cr, Mo, W, Tc, Re) species.

It may be of interest to mention the following results for the calculated D_0 values. Smaller vanadium species (VO_3) has larger D_0 (3.83 vs. 3.35 eV) than the larger one (V_3O_8), while the niobium and tantalum species have the opposite

Table 3 Energy (D_0 or ΔH_{0K} in eV) costs of oxygen atom loss from $M_xO_y^q$ ($\Delta = 1$) clusters by B3LYP

Group	$q = 0$ clusters	ΔH_{0K}	Group	$q = 1$	ΔH_{0K}	$q = -1$	ΔH_{0K}
3	$^2ScO_2 \rightarrow {}^2ScO + {}^3O$	3.97	3	$^2Sc_2O_3^+ \rightarrow {}^2Sc_2O_2^+ + {}^3O$	4.36	$^2Sc_2O_4^- \rightarrow {}^2Sc_2O_3^- + {}^3O$	4.39
	$^2YO_2 \rightarrow {}^2YO + {}^3O$	3.91		$^2Y_2O_3^+ \rightarrow {}^2Y_2O_2^+ + {}^3O$	4.58	$^2Y_2O_4^- \rightarrow {}^2Y_2O_3^- + {}^3O$	4.18
	$^2LaO_2 \rightarrow {}^2LaO + {}^3O$	4.02		$^2La_2O_3^+ \rightarrow {}^2La_2O_2^+ + {}^3O$	4.46	$^2La_2O_4^- \rightarrow {}^2La_2O_3^- + {}^3O$	4.01
	$^2Sc_3O_5 \rightarrow {}^2Sc_3O_4 + {}^3O$	4.61	4	$^2TiO_2^+ \rightarrow {}^2TiO^+ + {}^3O$	3.21	$^2TiO_3^- \rightarrow {}^2TiO_2^- + {}^3O$	4.84
	$^2Y_3O_5 \rightarrow {}^2Y_3O_4 + {}^3O$	4.27		$^2ZrO_2^+ \rightarrow {}^2ZrO^+ + {}^3O$	4.28	$^2ZrO_3^- \rightarrow {}^2ZrO_2^- + {}^3O$	4.42
	$^2La_3O_5 \rightarrow {}^2La_3O_4 + {}^3O$	4.12		$^2HfO_2^+ \rightarrow {}^2HfO^+ + {}^3O$	4.12	$^2HfO_3^- \rightarrow {}^2HfO_2^- + {}^3O$	4.40
5	$^2VO_3 \rightarrow {}^2VO_2 + {}^3O$	3.83		$^2Ti_2O_4^+ \rightarrow {}^2Ti_2O_3^+ + {}^3O$	3.40	$^2Ti_2O_5^- \rightarrow {}^2Ti_2O_4^- + {}^3O$	4.74
	$^2NbO_3 \rightarrow {}^2NbO_2 + {}^3O$	4.14		$^2Zr_2O_4^+ \rightarrow {}^2Zr_2O_3^+ + {}^3O$	4.08	$^2Zr_2O_5^- \rightarrow {}^2Zr_2O_4^- + {}^3O$	4.77
	$^2TaO_3 \rightarrow {}^2TaO_2 + {}^3O$	4.14		$^2Hf_2O_4^+ \rightarrow {}^2Hf_2O_3^+ + {}^3O$	4.15	$^2Hf_2O_5^- \rightarrow {}^2Hf_2O_4^- + {}^3O$	4.80
	$^2V_3O_8 \rightarrow {}^2V_3O_7 + {}^3O$	3.35		$^2Ti_3O_6^+ \rightarrow {}^2Ti_3O_5^+ + {}^3O$	3.49	$^2Ti_3O_7^- \rightarrow {}^2Ti_3O_6^- + {}^3O$	4.60
	$^2Nb_3O_8 \rightarrow {}^2Nb_3O_7 + {}^3O$	4.47		$^2Zr_3O_6^+ \rightarrow {}^2Zr_3O_5^+ + {}^3O$	4.40	$^2Zr_3O_7^- \rightarrow {}^2Zr_3O_6^- + {}^3O$	4.93
	$^2Ta_3O_8 \rightarrow {}^2Ta_3O_7 + {}^3O$	4.83		$^2Hf_3O_6^+ \rightarrow {}^2Hf_3O_5^+ + {}^3O$	4.64	$^2Hf_3O_7^- \rightarrow {}^2Hf_3O_6^- + {}^3O$	4.93
7	$^2TcO_4 \rightarrow {}^2TcO_3 + {}^3O$	3.33	5	$^2V_2O_5^+ \rightarrow {}^2V_2O_4^+ + {}^3O$	2.78	$^2V_2O_6^- \rightarrow {}^2V_2O_5^- + {}^3O$	3.90
	$^2ReO_4 \rightarrow {}^2ReO_3 + {}^3O$	3.84		$^2Nb_2O_5^+ \rightarrow {}^2Nb_2O_4^+ + {}^3O$	4.13	$^2Nb_2O_6^- \rightarrow {}^2Nb_2O_5^- + {}^3O$	4.79
	$^2Tc_3O_{11} \rightarrow {}^2Tc_3O_{10} + {}^3O$	1.90		$^2Ta_2O_5^+ \rightarrow {}^2Ta_2O_4^+ + {}^3O$	4.81	$^2Ta_2O_6^- \rightarrow {}^2Ta_2O_5^- + {}^3O$	5.06
	$^2Re_3O_{11} \rightarrow {}^2Re_3O_{10} + {}^3O$	2.61	6			$^2CrO_4^- \rightarrow {}^2CrO_3^- + {}^3O$	3.33
				$^2MoO_3^+ \rightarrow {}^2MoO_2^+ + {}^3O$	3.40	$^2MoO_4^- \rightarrow {}^2MoO_3^- + {}^3O$	4.29
				$^2WO_3^+ \rightarrow {}^2WO_2^+ + {}^3O$	3.71	$^2WO_4^- \rightarrow {}^2WO_3^- + {}^3O$	4.62
				$^2Mo_2O_6^+ \rightarrow {}^2Mo_2O_5^+ + {}^3O$	3.55	$^2Mo_2O_7^- \rightarrow {}^2Mo_2O_6^- + {}^3O$	3.18
				$^2W_2O_6^+ \rightarrow {}^2W_2O_5^+ + {}^3O$	4.28	$^2W_2O_7^- \rightarrow {}^2W_2O_6^- + {}^3O$	3.63
				$^2Mo_3O_9^+ \rightarrow {}^2Mo_3O_8^+ + {}^3O$	3.66	$^2Mo_3O_{10}^- \rightarrow {}^2Mo_3O_9^- + {}^3O$	2.98
				$^2W_3O_9^+ \rightarrow {}^2W_3O_8^+ + {}^3O$	4.25	$^2W_3O_{10}^- \rightarrow {}^2W_3O_9^- + {}^3O$	3.74
			7	$^2Tc_2O_7^+ \rightarrow {}^2Tc_2O_6^+ + {}^3O$	3.62	$^2Tc_2O_8^- \rightarrow {}^2Tc_2O_7^- + {}^3O$	2.65
				$^2Re_2O_7^+ \rightarrow {}^2Re_2O_6^+ + {}^3O$	3.13	$^2Re_2O_8^- \rightarrow {}^2Re_2O_7^- + {}^3O$	3.49

behavior (NbO_3/TaO_3/4.14 eV vs. Nb_3O_8/Ta_3O_8/4.47–4.83 eV). For the groups 4 and 5 metal species, each of the anionic clusters ($M_xO_y^-$, $\Delta = 1$) has a larger D_0 value than the corresponding cationic cluster ($M_xO_{y-1}^+$, $\Delta = 1$) does, such as $D_0(TiO_3^-) = 4.84$ eV vs. $D_0(TiO_2^+) = 3.21$ eV. However, this behavior (D_0 of anion $>D_0$ of cation) is not true or not always true for groups 3, 6, and 7 metal species. The D_0 value of $(TiO_2)_nTiO_3^-$ decreases as the cluster size increases ($n = 0$, 1, 2), while it is opposite for D_0 value of $(ZrO_2)_nZrO_3^-$ or $(HfO_2)_nHfO_3^-$. The D_0 of MO_4^- (group 6) increases and the one of MO_3^- (group 4) deceases as the M changes from 3d to 4d and to 5d metal atom.

4 Discussion

4.1 Comparison of the structures by B3LYP with those by BPW91 and others in literature

Figures 1, 4, and 6 indicate that the structures of these $\Delta = 1$ clusters by B3LYP are usually with low symmetries. For example, the C_s symmetry is determined for the ground state structures of MO_3 (M = V, Nb, Ta) and MO_3^+ (M = Cr, Mo, W) while the high symmetry of these clusters could be C_{3v} or D_{3h}. The pure GGA functional BPW91 is used to re-optimize the structures for most of the low-symmetry clusters in Figs. 1, 4, and 6. The results are as follows: ScO_2/C_{2v}, $^2B_2$; TiO_2^+/C_{2v}, $^2B_2$; ZrO_2^+/C_{2v}, $^2B_2$; TiO_3^-/D_{3h}, $^2A_2'$; HfO_3^-/C_{3v}, $^2A_2$; VO_3/C_{3v}, $^2A_2$; NbO_3/C_{3v}, $^2A_2$; TaO_3/C_{3v}, $^2A_2$; CrO_3^+/C_{3v}, $^2A_2$; MoO_3^+/C_{3v}, $^2A_2$; WO_3^+/C_{3v}, $^2A_2$; MoO_4^-/C_{2v}, $^2B_1$; WO_4^-/D_{2d}, $^2A_2$; TcO_4/C_{2v}, $^2B_1$; $V_2O_6^-/D_{2h}$, $^2B_{2u}$; $Nb_2O_6^-/D_{2h}$, $^2B_{1g}$; $Ta_2O_6^-/D_{2h}$, $^2B_{2u}$; $Mo_2O_6^+/D_{2h}$, $^2B_{1g}$; $W_2O_6^+/D_{2h}$, $^2B_{2u}$; $Mo_2O_7^-/D_{3d}$, $^2A_{2g}$; $W_2O_7^-/D_{3d}$, $^2A_{2g}$; $Tc_2O_7^+/D_{3d}$, $^2A_{2g}$; $Re_2O_7^+/D_3$, $^2A_1$; $Zr_3O_7^-/C_{3v}$, $^2A_1$; and Nb_3O_8/C_{2v}, $^2B_1$. It can be seen that high symmetries such as C_{3v} for MO_3 (M = V, Nb, Ta) and MO_3^+ (M = Cr, Mo, W) and D_{2h} for $V_2O_6^-$ are determined by BPW91. Because of high symmetry, the spin densities in each of the clusters optimized by BPW91 are significantly distributed over more than one terminal oxygen atoms (ranging from 0.2 to 0.5 μ_B). However, there is no experimental evidence that these BPW91 results are correct. On the contrary, the experiments on the infrared (IR) spectroscopy [114] indicated

that the high-symmetry structure of $V_2O_6^-/D_{2h}$ ($^2B_{2u}$) by BPW91 is wrong while the one [C_s ($^2A'$), Fig. 4] by B3LYP can be correct (see Fig. 5SI and the explanations in the supporting information for more details).

It has been realized in Refs. [71–74] that the symmetry breaking of the transition metal oxide cluster structures by B3LYP is due to the HF component in this hybrid functional. It is noticeable that for (pure) transition metal clusters in which the valence electron distributions have the delocalized nature the pure GGA functional (such as BPW91 for Nb_n [115]) usually has to be used, while these pure GGA functionals sometimes predict very poor results for transition metal oxide clusters (such as PBE for iron oxide clusters [62]) in which the metal atoms are in the high valence states (metal atoms are "well oxidized") and the valence electron distributions have the localized nature. It is also noticeable that the properties such as bond energy [116, 117], reactivity [41, 43, 45, 53, 54, 60, 118, 119], and IR spectroscopy [114, 120–122] of many "well oxidized" transition metal oxide clusters (or $\Delta \geq 0$ clusters) can be reasonably well predicted by the hybrid B3LYP functional which was originally developed and very suitable for main group species, in which the bonding (except for Π systems such as aromatics) is mostly localized in nature. With these considerations and the high symmetry for the selected cluster $V_2O_6^-$ by the pure GGA functional BPW91 is incorrect, we may conclude that the predictions by B3LYP in this study for the $\Delta = 1$ clusters are reasonable and useful, although further experiments and more reliable/expensive calculations are necessary for this system in future.

The structures of most of the mono-metal oxides (MO_y^q) were extensively studied in literature. The calculated ground state structures of the MO_{2-4}^q ($\Delta = 1$) clusters in Fig. 1 are generally in agreement with computational results in Refs. [123–131]. It is noticeable that for CrO_3^+, Ref. [132] predicted a ground state with three Cr–O_t bonds (see Fig. 2b) under B3LYP/LanL2DZ level, while this study predicts that the ground state has a η^2-O_2 unit under B3LYP/TZVP (see further discussion on CrO_3^+ in Sect. 4.3 below). The structures of the di- and tri-metal oxide clusters were relatively less studied. Our DFT structures of $M_{2,3}O_y^q$ ($\Delta = 1$) in Figs. 4 and 6 are also generally in agreement with available theoretical and experimental results in literature [41, 60, 129, 130, 133–139]. The structures of $Y_2O_3^+$ and $La_2O_3^+$ with three O_b atoms (Fig. 4) are similar to those predicted in Ref. [133]. The structures of $(ZrO_2)_{2-3}^+$ and $(ZrO_2)_{0-2}ZrO_3^-$ (Figs. 1, 4, 6) agree well with those by Johnson et al. [53, 60]. The structures of the vanadium oxide clusters were extensively studied by calculations and experiments [41, 45, 129, 134–138]. The results of VO_3, $V_2O_5^+$, $V_2O_6^-$, and V_3O_8 are the same as or similar to those in Refs. [41, 128, 129, 134–136]. The structures of $(MoO_3)_{1-3}^+$ clusters by us and by Oliveira et al. [130] are similar. The lowest energy structure of $W_3O_{10}^-$ (Fig. 6) is similar as the one reported in Ref. [139]. For $W_2O_7^-$ cluster (see Fig. 2f), the zero-point vibration corrected energy of the isomer with C_2 symmetry is lower by only 0.12 eV than that of the isomer with C_1 symmetry in this study. It is noticeable that if the zero-point vibration is not taken into account, the $W_2O_7^-$ isomer with C_1 symmetry is lower in energy by 0.03 eV than the one with C_2 symmetry in this study. The experimental and theoretical study in Ref. [140] supported that the $W_2O_7^-$ isomer with C_1 symmetry is the ground state and a high (D_{3d} in Ref. [140]) symmetry isomer is higher in energy by only 0.09 eV. Although the accuracy of the calculations in this study may not be high enough to determine the true ground states for clusters such as $Sc_2O_4^-$, $Hf_2O_4^+$, $Ti_2O_5^-$, $W_2O_7^-$, and $Ti_3O_6^+$ (see Fig. 2c–g) with isomers that are close (within 0.2 eV) in energy, these cluster isomers with slightly higher energy also contain radical oxygen $O^{\cdot}$.

4.2 Prediction and interpretation of the cluster reactivity

The DFT result that the studied $M_xO_y^q$ ($\Delta = 1$) clusters (Figs. 1, 4, 6, with a few exceptions that will be discussed in Sect. 4.3 below) contain radical oxygen $O^{\cdot}$ is generally consistent with the available experimental observations that $(V_2O_5)_{0-2}VO_3$ [37–39], $(V_2O_5)_{1-3}^+$ [40–46], $(MoO_3)_{1-3}^+$ [48, 50], TiO_2^+ [52], $(WO_3)_{1-3}^+$ [51], $(ZrO_2)_{1-4}^+$ [53, 61], $(ZrO_2)_{0-3}ZrO_3^-$ [60, 61], and $(V_2O_5)_{0-1}V_2O_6^-$ [58, 59] are highly reactive toward oxidation of hydrocarbons, monoxide, and so on. On the basis that the above consistency generally validates the adopted computational method, this study predicts that a lot of other TMO clusters may be with high oxidative reactivity. For examples, (1) $(TiO_2)_{1-3}^+$ clusters may be more oxidative than $(ZrO_2)_{1-3}^+$, since the former have smaller D_0 values than the latter do; (2) the highly reactive clusters identified in previous experiments are all with $O_t^{\cdot}$, it is interesting to carry out reactivity experiments on $M_2O_3^+$ (group 3, Fig. 4), $(Sc_2O_3)_{2,3}^+$ (Fig. 8), or similar clusters with $O_b^{\cdot}$; and (3) there were very limited experimental data on neutral [37–39] and anionic [58–61] TMO clusters with high oxidative reactivity, this study predicts that $(Re_2O_7)_{n=0,1}ReO_4$, $(MoO_3)_{n=1,2}MoO_4^-$, and $(WO_3)_{n=1,2}WO_4^-$ with low D_0 values (2.61–3.84 eV, see Table 3) are potential candidates for experimental investigations.

Table 3 shows that the D_0 values of $M_xO_y^q$ ($\Delta = 1$) depends strongly on the metal atom, cluster size, composition, and charge state. In the absence of any information of reaction kinetics, the calculated D_0 values may be used to quickly interpret the observed cluster reactivity in more details from a consideration of thermodynamics. Recent

experiments indicated that reactions of $(ZrO_2)_{1-4}^+$ with CO, C_2H_4, and C_2H_2 produce CO_2, C_2H_4O, and C_2H_2O, respectively, and $Zr_2O_4^+$ cluster is relatively more reactive than ZrO_2^+ and $Zr_3O_6^+$ [53]. This can be rationalized by using the smaller D_0 value of $Zr_2O_4^+$ (4.08 eV) than those of ZrO_2^+ (4.28 eV) and $Zr_3O_6^+$ (4.40 eV) (see Table 3). Experiments on the reactivity of $(ZrO_2)_{0-3}ZrO_3^-$ toward CO [60, 61] measured that the reaction rate constant of ZrO_3^- + CO is 2.1 × 10^{-12} cm^3 s^{-1} and those of $Zr_2O_5^-$/$Zr_3O_7^-$ + CO is on the order of 10^{-13} cm^3 s^{-1}. Our calculations indicate that the D_0 value of ZrO_3^- (4.42 eV) is smaller than those of $Zr_2O_5^-$ (4.77 eV) and $Zr_3O_7^-$ (4.93 eV), which is again in consistent with the experiments. It is noticeable that the calculated D_0(O–CO) is 5.50 eV and the reactions of ZrO_3^-, $Zr_2O_5^-$, and $Zr_3O_7^-$ with CO to form CO_2 release, respectively, the energies of 1.08, 0.73, and 0.57 eV of which the difference can be considered significant. This may well explain the higher reactivity of ZrO_3^- over $Zr_3O_7^-$ in the reaction with CO. The lower or non-reactivity of the 4d/5d metal species $(ZrO_2)_{1-4}^+$ and $(ZrO_2)_{0-3}ZrO_3^-$ [53, 60, 61], $(Nb_2O_5)_{1-3}^+$ and $(Ta_2O_5)_{1-3}^+$ [47, 141, 142], $(Nb_2O_5)_{0-2}NbO_3$ [39] versus that of the 3d metal species $[(V_2O_5)_{1-3}^+$ [40–43] and $(V_2O_5)_{0-2}VO_3$ [37–39] by experiments can also be rationalized with the lower D_0 values of the latter clusters than those of the former ones (>4 eV).

It is interesting to compare the reactivity of O˙ over transition metal oxide clusters with those of other oxygen-based radicals such as HO and NO_3 that have been extensively studied by experiments and theoretical calculations [143–146]. It was reported that the reaction of OH with CH_4 needs to overcome 6.1–7.9 kcal/mol barrier (when the zero-point energy is included, the values range from 4.7 to 6.6 kcal/mol) and the rate constant is about 7.89 × 10^{-15} cm^3 $molecule^{-1}$ s^{-1}. The rate constants for hydrogen atom abstraction from alkane molecules by NO_3 radical are reported to be on the order of 10^{-17} cm^3 $molecule^{-1}$ s^{-1}. The transition metal oxide cluster cations with O˙ are generally much more reactive than OH and NO_3 toward hydrocarbon molecules. The rate constants for hydrogen atom abstraction from CH_4 by $V_4O_{10}^+$ [45], TiO_2^+ [52], and ZrO_2^+ [52] are reported to be (5.5 ± 0.69) × 10^{-10}, 7.4 × 10^{-11}, and 3.7 × 10^{-11} cm^3 $molecule^{-1}$ s^{-1}, respectively. Recently, we identified the hydrogen atom abstraction from C_2H_6 and C_4H_{10} molecules by the anionic cluster $Zr_2O_5^-$ that is with O˙, and the estimated rate constants are 4 × 10^{-12} and 2 × 10^{-11} cm^3 $molecule^{-1}$ s^{-1}, respectively [147]. So far, there is no experimental report on the rate constants for reactions of neutral transition metal oxide clusters with O˙ toward reactants such as hydrocarbon molecules. The theoretical calculations on VO_3 + C_2H_4 [37], VO_3 + C_3H_6 [118], and V_3O_8 + C_2H_4 [148] indicated that the oxidation of these alkene molecules by VO_3 and V_3O_8 that are with O˙ is overall barrierless.

4.3 V–Mo–Re diagonal line

Among the studied $M_xO_y^q$ (M are the 3d–5d metals in groups 3–7) clusters we find that only $Cr_xO_y^q$ (except for CrO_4^-) and $Mn_xO_y^q$ clusters have [O–O] unit. This result may be rationalized by the small D_0 values of CrO (4.78 eV [85]) and MnO (3.83 eV [85]) listed in Table 2. The binding energies of oxygen atom with $M_xO_{y-1}^q$ ($\Delta = -1$) clusters can be denoted as $D_0(\Delta = 1)$. Because the metal atoms in $\Delta = -1$ clusters are in or close to the high valence states, less energy can be released in the oxidation of the $\Delta = -1$ clusters by O atom than in the oxidation of the corresponding metal atoms (M). As a result, the $D_0(\Delta = 1)$ listed in Table 3 are smaller than the calculated $D_0(MO)$ in Table 2 significantly. For example, the $D_0(\Delta = 1)$ of cationic clusters are smaller than the corresponding $D_0(MO)$ values by more than 2.3, 3.2, 3.0, 1.6, and 1.7 eV for groups 3, 4, 5, 6, and 7 metal species, respectively. In the case that $D_0(\Delta = 1)$ is too small, the last oxygen atom bonded with the $\Delta = -1$ (CrO_2^+) cluster (to form $\Delta = 1$) may have significant bonding with an oxygen atom to form O–O unit because the oxygen–oxygen bond is quite strong ($D_0(O_2)$ = 5.12 eV [88]). This rationalizes that there is one O–O unit in the chromium and manganese $\Delta = 1$ clusters such as CrO_3^+ and MnO_4, since D_0(CrO) and D_0(MnO) are the smallest among $D_0(MO)$ in Table 2. It is noticeable that the photoelectron spectroscopic and computational study on MO_y^- (M = Cr, Mo, W) identified that the bonding properties of WO_4 (and possibly MoO_4) are quite different from those of CrO_4, which can also be traced back to the larger D_0 of WO (and MoO) over that of CrO [123, 124].

Figure 2 indicates that the CrO_3^+ isomer with O˙ (and without O–O) is the ground state under BPW91 while it is the excited state under B3LYP. Figure 6SI shows the reaction pathways for CH_4 reaction with CrO_3^+ cluster that contains O˙. The reaction ($CrO_3^{+\cdot}$ + CH_4 → CrO_3H^+ + $CH_3^{\cdot}$) is overall barrierless and would be experimentally observed in the case that there is an O˙ in the cluster (no matter B3LYP or BPW91 is used). However, recent cluster reactivity experiments [149] indicate that the hydrogen abstraction from CH_4 by CrO_3^+ (or $Cr_2O_6^+$) was not experimentally observed, indicating that the BPW91 prediction of the ground electronic structure of CrO_3^+ is wrong while the B3LYP ground state (with O–O, lower symmetry) is acceptable. In contrast, the experiments indicate that MoO_3^+, WO_3^+, $Mo_2O_6^+$, and $W_2O_6^+$ clusters can abstract a hydrogen atom from CH_4 at near room temperature conditions although Cr, Mo, and W are in the same group 6 in the periodic table. It should be pointed out that, under B3LYP, there is no O–O unit in the ground states of neutral CrO_3 and anionic CrO_3^- while there

is one such O–O unit in CrO_3^+, indicating the charge-dependence of the cluster structures [62].

The current DFT study suggests that chromium and manganese of the 3d transition metals do not belong to the type of transition metals (denoted as M/O$^{\cdot}$ in the text below), of which all of the oxide clusters in the form of $M_xO_y^q$ ($\Delta = 1$) contains radical oxygen. In contrast, two more 4d (Mo and Tc) and 5d (W and Re) metals belong to M/O$^{\cdot}$. This is also in parallel with the relatively large D_0 of Mo–O (5.44 eV [87]), Tc–O (5.64 eV [88]), W–O (7.01 eV [92]), and Re–O (6.46 eV [88]). Our recent experimental investigations [149] on the reactions of cationic $Cr_xO_y^+$, $Mo_xO_y^+$, $W_xO_y^+$, $Mn_xO_y^+$, and $Re_xO_y^+$ clusters toward CH_4 have identified that $(MoO_3)_{1-2}^+$, $(WO_3)_{1-3}^+$, and $Re_2O_7^+$ clusters can activate CH_4 under near room temperature conditions, in agreement with the DFT results that these clusters contain reactive O$^{\cdot}$ atoms. In sharp contrast, there is no evidence of CH_4 activation by $(CrO_3)_{1-3}^+$ and $Mn_2O_7^+$ in the experiments, which can be rationalized by the B3LYP results that there is no O$^{\cdot}$ atom in these clusters. If we neglect the technetium which is a radioactive element (with no stable isotope), a diagonal line can be drawn over V, Mo, and Re for the 3d–5d transition metals in the periodic table. The DFT study predicts that all of the 3d–5d transition metals on the bottom-left side of the V–Mo–Re line (included) belong to M/O$^{\cdot}$. It is likely that most of the transition metals on the top-right side of the line do not belong to M/O$^{\cdot}$. Our test calculations at B3LYP level indicate that MO_4^+ and MO_5^- (M = Fe, Ru in group 8) clusters which are $\Delta = 1$ according to the definition in the Introduction section are with one or two O–O moieties. In contrast, OsO_4^+ and OsO_5^- clusters are predicted by B3LYP to have four and five O_t atoms, respectively, and contain the radical oxygen $O_t^{\cdot}$. The results of OsO_4^+ and OsO_5^- are consistent with the large D_0 (6.16 eV) [88] value of OsO.

4.4 Isoelectronic clusters

The neutral cluster systems MO_2 (group 3) and MO_3 (group 5) have the same total number of valence (metal valence d and s plus oxygen 2s and 2p) electrons as the charged species MO_2^+ (group 4) and MO_3^- (group 4), respectively. Figures 1 and 3 indicate that these isoelectronic clusters have similar geometries and SOMO distributions. All of the di-metal $M_2O_y^q$ clusters with $\Delta = 1$ (Fig. 4) are charged species. Since the isoelectronic clusters (Figs. 1, 3) have similar bonding properties, it is therefore possible to find neutral mixed-di-metal clusters $M'M''O_y$ that have similar bonding properties to those positively and negatively charged clusters in Figs. 4 and 5. For example, we have tested that the bonding properties of $TiVO_5$ and $CrVO_6$ are similar to those of $V_2O_5^+$ and $V_2O_6^-$, respectively. This kind of metal atom substitution may also be applied to tri-metal and large multi-metal species for interchange of the charged oxide clusters with the neutral ones. The substitution will tune the cluster reactivity from considerations of both thermodynamics and kinetics, which may be further investigated by both theory and experiment.

4.5 A reconsideration of radical oxygen in condensed phase catalysis

The investigations reported in literature have demonstrated that the radical oxygen plays an important role in several useful reactions, for example, the selective conversion of methane to methanol and formaldehyde using N_2O as oxidant [16–20, 22], dehydrogenation of ethane to produce ethylene [21], oxidation of benzene to phenol with high selectivity [150], and partial oxidation of propylene to acrolein [118, 151]. These processes were facilitated by V_2O_5/SiO_2 or MoO_3/SiO_2 catalysts. The $V_xO_y^q$ ($\Delta = 1$) and $Mo_xO_y^q$ ($\Delta = 1$) clusters with $O_t^{\cdot}$ in this study represent possible candidates for the chemical structures of radical oxygen over MoO_3/SiO_2 and V_2O_5/SiO_2 surfaces. We propose that the surface radical oxygen (O$^{\cdot}$) can be chemically bonded as $(O_b)_2VO_tO_t^{\cdot}$ ($V_2O_5^+$ in Fig. 5), $(O_b)_2V(O_tO_t)^{\cdot}$ ($V_2O_6^-$/Fig. 5, V_3O_8/Fig. 7), $(O_b)_2MoO_tO_t^{\cdot}$ ($Mo_2O_6^+$/Fig. 5, $Mo_3O_9^+$/Fig. 7), or $O_bMo(O_t)_2O_t^{\cdot}$ ($Mo_2O_7^-$/Fig. 5, $Mo_3O_{10}^-$/Fig. 7), in which the bridging O_b atom is also bonded with surface support atom Si as well as V or Mo depending on the load of the metal in the catalysts.

This study predicts that the existence of radical oxygen in TMO clusters is common. That is, for any transition metals on the bottom-left side of V-Mo-Re in the periodic table, the oxide clusters $M_xO_y^q$ ($\Delta = 1$) are able to contain $O_t^{\cdot}$ or $O_b^{\cdot}$. This implies that it is possible to develop new (other than V [20, 22] and Mo [16–19, 21]) metal (or mixed metals through doping [152–155])-based oxide catalysts to supply radical oxygen for oxidation reactions.

The obvious advantage of using radical oxygen for oxidation reactions is that the activation of the reacting molecules (such as CH activation of CH_4 [45]) and the oxygen transfer from the catalyst to the target molecules can be with very small apparent positive or even large apparent negative activation energies (E_0), as what have been revealed by the theoretical and experimental cluster reactivity studies [37–46, 118, 156, 157]. The disadvantage of using radical oxygen may be its low concentrations. For example, the surface species $(O_b)_3VO_t$ [see Fig. 7 for $(O_b)_3VO_t$ moieties in V_3O_8] may be much more stable than $(O_b)_2VO_tO_t^{\cdot}$, so the concentration of the latter [$C(O_t^{\cdot})$] should be much lower than that of the former [$C(O_t)$] over a practically prepared catalyst. In a unit time, the number (N) of converted molecules (such as $CH_4 \rightarrow CH_3OH$) over a TMO surface may be

simply (for comparison below, other unimportant factors neglected) written as $N(O_t^{\cdot}) = C(O_t^{\cdot}) \times \exp[-E_0(O_t^{\cdot})/k_BT]$ and $N(O_t) = C(O_t) \times \exp[-E_0(O_t)/k_BT]$ for conversions over $(O_b)_2VO_tO_t^{\cdot}$ and $(O_b)_3VO_t$ sites, respectively, in which k_B is the Boltzmann constant and T is the temperature. To find the relative value of $C(O_t^{\cdot})/C(O_t)$ that satisfies $N(O_t^{\cdot}) = N(O_t)$, we assume $E_0(O_t^{\cdot}) = 0$, $E_0(O_t) = 2$ eV (typical value of CH activation over VO_t sites) [158, 159], and $k_BT = 0.0431$ eV ($T = 500$ K). With the above equations and parameters, $C(O_t^{\cdot})/C(O_t) = \exp\{[E_0(O_t^{\cdot})–E_0(O_t)]/k_BT\} = e^{-46.4} \approx 10^{-20}$ is obtained. This means that the conversion over the radical oxygen sites may be efficient enough (comparable with the conversion over "normal" sites) even the radical oxygen is with too low concentration to be detected by standard surface characterization methods. The above estimation further implies that it is important to study cluster systems to understand the nature of radical oxygen in condensed phase catalysis.

5 Conclusions

The structure and bonding properties of groups 3–7 transition metal oxide clusters $M_{x=1-3}O_y^q$ and $Sc_{x=4-6}O_y^q$ with $\Delta = 2y - nx + q = 1$ (n is the number of metal valence electrons and q is the charge number) are studied by the DFT calculations. The DFT results are generally supported by the available experimental and theoretical studies in literature. The existence of oxygen radical [$O^{\cdot}$ with the unpaired electron being localized on the oxygen 2p orbital(s)] in the $M_xO_y^q$ ($\Delta = 1$) clusters is common. All of the 3d–5d metals on the bottom-left side of the V–Mo–Re diagonal line in the periodic table belong to the type of metals of which all of the $M_xO_y^q$ ($\Delta = 1$) clusters contain $O^{\cdot}$. $Cr_xO_y^q$ ($\Delta = 1$, except CrO_4^-) and $Mn_xO_y^q$ ($\Delta = 1$) do not contain $O^{\cdot}$ at the B3LYP level. Most of the clusters have one or two terminal oxygen atoms as the radical oxygen while some of the $M_xO_y^q$ ($\Delta = 1$, M = Sc, Y, La) clusters are with one or two bridging oxygen atoms as the radical oxygen. The oxide clusters of 3d (Sc and Ti) and V–Mo–Re metals have relatively high oxidative reactivity due to the relatively small (typically 3–4 eV) energy costs of oxygen atom loss from the $M_xO_y^q$ ($\Delta = 1$) clusters. Mixed-metal oxide clusters (such as $TiVO_5$ and $CrVO_6$) with radical oxygen can also be derived by appropriate counting of the total number of metal valence electrons and the number of oxygen atoms in the systems. This study suggests possible chemical structures for radical oxygen over V_2O_5/SiO_2 and MoO_3/SiO_2 catalysts and the possibility to develop other catalysts to supply radical oxygen for oxidation reactions. The high reactivity of the radical oxygen may be able to balance its low concentration in the condensed phase catalysis.

Acknowledgments This work was supported by the Chinese Academy of Sciences (Hundred Talents Fund), the National Natural Science Foundation of China (Nos. 20703048, 20803083, and 20933008), and the 973 Program (No. 2006CB932100).

References

1. Barteau MA (1996) Chem Rev 96:1413
2. Fierro GJL (2006) Metal oxides chemistry and applications. Taylor & Francis, London
3. Surnev S, Ramsey MG, Netzer FP (2003) Prog Surf Sci 73:117
4. Bell AT (2003) Science 299:1688
5. Martinez-Huerta MV, Gao X, Tian H, Wachs IE, Fierro JLG, Banares MA (2006) Catal Today 118:279
6. Li M, Shen J (2002) J Catal 205:248
7. Zhao C, Wachs IE (2006) Catal Today 118:332
8. Dunn JP, Stenger HG, Wachs IE (1999) Catal Today 51:301
9. Yamazoe S, Masutani Y, Teramura K, Hitomi Y, Shishido T, Tanaka T (2008) Appl Catal B Environ 83:123
10. Gabasch H, Knop-Gericke A, Schlögl R, Borasio M, Weilach C, Rupprechter G, Penner S, Jenewein B, Hayeka K, Klötzer B (2007) Phys Chem Chem Phys 9:533
11. Alvarez-Merino MA, Ribeiro MF, Silva JM, Carrasco-Marn F, Maldonado-Hdar FJ (2004) Environ Sci Technol 38:4664
12. Seiyama T, Nita K, Maehara T, Yamazoe N, Takita Y (1997) J Catal 49:164
13. Ushikubo T (2000) Catal Today 57:331
14. Shvets VA, Kazansky VB (1972) J Catal 25:123
15. Ben TY, Lunsford JH (1973) Chem Phys Lett 19:348
16. Liu RS, Iwamoto M, Lunsford JH (1982) J Chem Soc Chem Commun 78
17. Lipatkina NI, Shvets VA, Kazansky VB (1978) Kinet Katal 19:979
18. Liu HF, Liu RS, Liew KY, Johnson RE, Lunsford JH (1984) J Am Chem Soc 106:4117
19. Khan MM, Somorjai GA (1985) J Catal 91:263
20. Zhen KJ, Khan MM, Mak CH, Lewis KB, Somorjai GA (1985) J Catal 94:501
21. Ward MB, Lin MJ, Lunsford JH (1977) J Catal 50:306
22. Launay H, Loridant S, Nguyen DL, Volodin AM, Dubois JL, Millet JMM (2007) Catal Today 128:176
23. Parfenov MV, Starokon EV, Semikolenov SV, Panov GI (2009) J Catal 263:173
24. Chernyavsky VS, Pirutko LV, Uriarte AK, Kharitonov AS, Panov GI (2007) J Catal 245:466
25. Dubkov KA, Ovanesyan NS, Shteinman AA, Starokon EV, Panov GI (2002) J Catal 207:341
26. Yuranov I, Bulushev DA, Renken A, Kiwi-Minsker L (2007) Appl Catal A 319:128
27. Schröder D, Schwarz H (1995) Angew Chem Int Ed 34:1973
28. Johnson JRT, Panas I (2000) Inorg Chem 39:3192
29. Waters T, O'Hair RAJ, Wedd AG (2003) J Am Chem Soc 125:3384
30. Justes DR, Moore NA, Castleman AW Jr (2004) J Phys Chem B 108:3855
31. Fu G, Xu X, Wan HL (2006) Catal Today 117:133
32. Feyel S, Scharfenberg L, Daniel C, Hartl H, Schröder D, Schwarz H (2007) J Phys Chem A 111:3278

33. Wang ZC, Ding XL, Ma YP, Cao H, Wu XN, Zhao YX, He SG (2009) Chin Sci Bull 54:2814
34. Ma YP, Xue W, Wang ZC, Ge MF, He SG (2008) J Phys Chem A 112:3731
35. Ding XL, Xue W, Ma YP, Zhao YX, Wu XN, He SG (2010) J Phys Chem C 114:3161
36. Li HB, Tian SX, Yang JL (2009) Chem Eur J 41:10747
37. Dong F, Heinbuch S, Xie Y, Rocca JJ, Bernstein ER, Wang ZC, Deng K, He SG (2008) J Am Chem Soc 130:1932
38. He SG, Xie Y, Dong F, Heinbuch S, Jakubikova E, Rocca JJ, Bernstein ER (2008) J Phys Chem A 112:11067
39. Dong F, Heinbuch S, Xie Y, Bernstein ER, Rocca JJ, Wang ZC, Ding XL, He SG (2009) J Am Chem Soc 131:1057
40. Zemski KA, Justes DR, Castleman AW Jr (2001) J Phys Chem A 105:10237
41. Justes DR, Mitrić R, Moore NA, Bonačić-Koutecký V, Castleman AW Jr (2003) J Am Chem Soc 125:6289
42. Justes DR, Castleman AW Jr, Mitrić R, Bonačić-Koutecký V (2003) Eur Phys J D 24:331
43. Moore NA, Mitrić R, Justes DR, Bonačić-Koutecký V, Castleman AW Jr (2006) J Phys Chem B 110:3015
44. Bell RC, Zemski KA, Kerns KP, Deng HT, Castleman AW Jr (1998) J Phys Chem A 102:1733
45. Feyel S, Döbler J, Schröder D, Sauer J, Schwarz H (2006) Angew Chem Int Ed 45:4681
46. Feyel S, Schröder D, Schwarz H (2006) J Phys Chem A 110:2647
47. Zemski KA, Justes DR, Castleman AW Jr (2002) J Phys Chem B 106:6136
48. Kretzschmar I, Fiedler A, Harvey JN, Schröder D, Schwarz H (1997) J Phys Chem A 101:6252
49. Irikura KK, Beauchamp JL (1989) J Am Chem Soc 111:75
50. Fialko EF, Kikhtenko AV, Goncharov VB, Zamaraev KI (1997) J Phys Chem A 101:8607
51. Johnson GE, Tyo EC, Castleman AW Jr (2008) Proc Natl Acad Sci USA 105:18108
52. Harvey JN, Diefenbach M, Schröder D, Schwarz H (1999) Int J Mass Spectrom 182/183:85
53. Johnson GE, Mitrić R, Tyo EC, Bonačić-Koutecký V, Castleman AW Jr (2008) J Am Chem Soc 130:13912
54. Wu XN, Zhao YX, He SG, Ding XL (2009) Chin J Chem Phys 22:635
55. Schröder D, Roithová J (2006) Angew Chem Int Ed 45:5705
56. Feyel S, Döbler J, Höckendorf R, Beyer MK, Sauer J, Schwarz H (2008) Angew Chem Int Ed 47:1946
57. Sierka M, Döbler J, Sauer J, Santambrogio G, Brümmer M, Wöste L, Janssens E, Meijer G, Asmis KR (2007) Angew Chem Int Ed 46:3372
58. Bell RC, Castleman AW Jr (2002) J Phys Chem A 106:9893
59. Li SH, Mirabal A, Demuth J, Wöste L, Siebert T (2008) J Am Chem Soc 130:16832
60. Johnson GE, Mitrić R, Nössler M, Tyo EC, Bonačić-Koutecký V, Castleman AW Jr (2009) J Am Chem Soc 131:5460
61. Johnson GE, Mitrić R, Bonačić-Koutecký V, Castleman AW Jr (2009) Chem Phys Lett 475:1
62. Xue W, Yin S, Ding XL, He SG, Ge MF (2009) J Phys Chem A 113:5302
63. Frisch MJ, Trucks GW, Schlegel HB, Scuseria GE, Robb MA, Cheeseman JR, Montgomery JA Jr, Vreven T, Kudin KN, Burant JC, Millam JM, Iyengar SS, Tomasi J, Barone V, Mennucci B, Cossi M, Scalmani G, Rega N, Petersson GA, Nakatsuji H, Hada M, Ehara M, Toyota K, Fukuda R, Hasegawa J, Ishida M, Nakajima T, Honda Y, Kitao O, Nakai H, Klene M, Li X, Knox JE, Hratchian HP, Cross JB, Adamo C, Jaramillo J, Gomperts R, Stratmann RE, Yazyev O, Austin AJ, Cammi R, Pomelli C, Ochterski JW, Ayala PY, Morokuma K, Voth GA, Salvador P, Dannenberg JJ, Zakrzewski VG, Dapprich S, Daniels AD, Strain MC, Farkas O, Malick DK, Rabuck AD, Raghavachari K, Foresman JB, Ortiz JV, Cui Q, Baboul AG, Clifford S, Cioslowski J, Stefanov BB, Liu G, Liashenko A, Piskorz P, Komaromi I, Martin RL, Fox DJ, Keith T, Al-Laham MA, Peng CY, Nanayakkara A, Challacombe M, Gill PM W, Johnson B, Chen W, Wong MW, Gonzalez C, Pople JA (2004) Gaussian 03, Revision B.05. Gaussian Inc, Wallingford
64. Becke AD (1988) Phys Rev A 38:3098
65. Becke AD (1993) J Chem Phys 98:5648
66. Lee C, Yang W, Parr RG (1988) Phys Rev B 37:785
67. Schäfer A, Huber C, Ahlrichs R (1994) J Chem Phys 100:5829
68. Andrae D, Haeussermann U, Dolg M, Stoll H, Preuss H (1990) Theor Chim Acta 77:123
69. Weigend F, Ahlrichs R (2005) Phys Chem Chem Phys 7:3297
70. Glendening ED, Reed AE, Carpenter JE, Weinhold F, NBO, version 3.1
71. Li S, Dixon DA (2006) J Phys Chem A 110:6231
72. Li S, Dixon DA (2007) J Phys Chem A 111:11908
73. Zhai HJ, Li S, Dixon DA, Wang LS (2008) J Am Chem Soc 130:5167
74. Li S, Zhai HJ, Wang LS, Dixon DA (2009) J Phys Chem A 113:11273
75. Li S, Dixon DA (2007) J Phys Chem A 111:11093
76. Li S, Hennigan JM, Dixon DA, Peterson KA (2009) J Phys Chem A 113:7861
77. Perdew JP, Wang Y (1991) Phys Rev B 45:13244
78. Raghavachari K, Trucks GW, Pople JA, Head-Gordon M (1989) Chem Phys Lett 157:479
79. Watts JD, Gauss J, Bartlett RJ (1993) J Chem Phys 98:8718
80. Lee TJ, Taylor PR (1989) Int J Quantum Chem S23:199
81. Huber K, Herzberg G (1979) Molecular spectra and molecular structure IV. Constants of Diatomic Molecules. Van Nostrand Rheinhold, NewYork. See also Chemistry Webbook from the NIST website (http://nist.gov/)
82. Gordon RM, Merer AJ (1980) Can J Phys 58:642
83. Hamrick YM, Taylor S, Morse MD (1991) J Mol Spectrosc 146:274
84. Yao C, Guan W, Song P, Su ZM, Feng JD, Yan LK, Wu ZJ (2007) Theor Chem Acc 117:115
85. Gutsev GL, Andrews L, Bauschlicher CW Jr (2003) Theor Chem Acc 109:298
86. Song P, Guan W, Yao C, Su ZM, Wu ZJ, Feng JD, Yan LK (2007) Theor Chem Acc 117:407
87. Loocka HP, Simard B, Wallin S, Linton C (1998) J Chem Phys 109:8980
88. Pedley JB, Marshall EM (1983) J Phys Chem Ref Data 12:967
89. Gole JL, Chalek CL (1976) J Chem Phys 65:4384
90. Ackermann RJ, Rauh EG (1974) J Chem Phys 60:2266
91. Smoes S, Drowart J, Myers CE (1976) J Chem Thermody 8:225
92. Hinton CS, Li FX, Armentrout PB (2009) Int J Mass Spectrom 280:226
93. Clemmer DE, Elkind JL, Aristov N, Armentrout PB (1991) J Chem Phys 95:3387
94. Harrington J, Weisshaar JC (1992) J Chem Phys 97:2809
95. Dyke JM, Gravenor BWJ, Lewis RA, Morris A (1983) J Chem Soc Faraday Trans 79:2083
96. Armentrout PB, Halle LF, Beauchamp JL (1982) J Chem Phys 76:2449
97. Rauh EG, Ackermann RJ (1974) J Chem Phys 60:1396
98. Rauh EG, Ackermann RJ (1975) J Chem Phys 62:1584
99. Merritt JM, Bondybey VE, Heaven MC (2009) J Chem Phys 109:8980
100. Dyke JM, Ellis AM, Feher M, Morris A, Paul AJ, Stevens JCH (1987) J Chem Soc Faraday Trans 83:1555

101. Tonkyn RG, Winniczek JW, White MG (1989) Chem Phys Lett 164:137
102. Wu HB, Wang LS (1998) J Phys Chem A 102:9129
103. Thomas OC, Xu SJ, Lippa TP, Bowen KH (1999) J Cluster Sci 10:525
104. Green SME, Alex S, Fleischer NL, Millam EL, Marcy TP, Leopoldf DG (2001) J Chem Phys 114:2653
105. Gunion RF, Dixon-Warren SJ, Lineberger WC (1996) J Chem Phys 104:1765
106. Zheng WJ, Li X, Eustis S, Bowen K (2008) Chem Phys Lett 130:144503
107. Ervin KM, Anusiewicz W, Skurski P, Simons J, Lineberger WC (2003) J Phys Chem A 107:8521
108. Li S, Dixon DA (2008) J Phys Chem A 112:6646
109. Vyboishchikov SF, Sauer J (2001) J Phys Chem A 105:8588
110. Ding XL, Xue W, Ma YP, Wang ZC, He SG (2009) J Chem Phys 130:014303
111. Dong F, Heinbuch S, He SG, Xie Y, Rocca JJ, Bernstein ER (2006) J Chem Phys 125:164318
112. Balducci G, Gigli G, Guido M (1981) J Chem Soc Faraday Trans II 77:1107
113. Zhai HJ, Wang LS (2008) J Am Chem Soc 2007 129:3022
114. Asmis KR, Sauer J (2007) Mass Spectrom Rev 26:542
115. Xie Y, He SG, Dong F, Bernstein ER (2008) J Chem Phys 128:044306
116. Calatayud M, Silvi B, Andrés J, Beltrán A (2001) Chem Phys Lett 333:493
117. Gong Y, Zhou MF (2009) Chem Rev 109:6765
118. Wang ZC, Xue W, Ma YP, Ding XL, He SG, Dong F, Heinbuch S, Rocca JJ, Bernstein ER (2008) J Phys Chem A 112:5984
119. Xue W, Wang ZC, He SG, Xie Y, Bernstein ER (2008) J Am Chem Soc 130:15879
120. Rozanska X, Fortrie R, Sauer J (2007) J Phys Chem C 111:6041
121. Fielicke A, Meijer G, von Helden G (2003) J Am Chem Soc 125:3659
122. Brümmer M, Kaposta C, Santambrogio G, Asmis KR (2003) J Chem Phys 119:12700
123. Gutsev GL, Jena P, Zhai HJ, Wang LS (2001) J Chem Phys 115:7935
124. Zhai HJ, Kiran B, Cui LF, Li X, Dixon DA, Wang LS (2004) J Am Chem Soc 126:16134
125. Uzunova EL, Mikosch H, Nikolov GS (2008) J Chem Phys 128:094307
126. Andrews L, Zhou MF, Chertihin GV, Bauschlicher CW Jr (1999) J Phys Chem A 103:6525
127. Lee EPF, Dyke JM, Mok DKW, Chau FT (2008) J Phys Chem A 112:4511
128. Calatayud M, Silvi B, Andrés J, Beltrán A (2001) Chem Phys Lett 333:493
129. Vyboishchikov SF, Sauer J (2000) J Phys Chem A 104:10913
130. Oliveira JA, Almeida WBD, Duarte HA (2003) Chem Phys Lett 372:650
131. Gong Y, Wang GJ, Zhou MF (2008) J Phys Chem A 112:4936
132. Molek KS, Reed ZD, Ricks AM, Duncan MA (2007) J Phys Chem A 111:8080
133. Reed ZD, Duncan MA (2008) J Phys Chem A 112:5354
134. Asmis KR, Meijer G, Brümmer M, Kaposta C, Santambrogio G, Wöste L, Sauer J (2004) J Chem Phys 120:6461
135. Jakubikova E, Rappé AK, Bernstein ER (2007) J Phys Chem A 111:12938
136. Zhai HJ, Wang LS (2002) J Chem Phys 117:7882
137. Santambrogio G, Brümmer M, Wöste L, Döbler J, Sierka M, Sauer J, Meijer G, Asmis KR (2008) Phys Chem Chem Phys 10:3992
138. Knight LB Jr, Babb R, Ray M, Banisaukas TJ, Russon L, Dailey RS, Davidson ER (1996) J Chem Phys 105:10237
139. Huang X, Zhai HJ, Li J, Wang LS (2006) J Phys Chem A 110:85
140. Zhai HJ, Huang X, Waters T, Wang XB, O'Hair RAJ, Wedd AG, Wang LS (2005) J Phys Chem A 109:10512
141. Zemski KA, Justes DR, Bell RC, Castleman AW Jr (2001) J Phys Chem A 105:4410
142. Zemski KA, Bell RC, Castleman AW Jr (2000) J Phys Chem A 104:5732
143. Espinosa-García J, Corchado JC (2000) J Chem Phys 112:5731
144. Fokin AA, Schreiner PR (2002) Chem Rev 102:1551
145. Sander, SP, Friedl RR, Ravishankara AR, Golden DM, Kolb CE, Kurylo MJ, Huie RE, Orkin VL, Molina MJ, Moortgat GK, Finlayson-Pitts BJ (2003) Chemical kinetics and photochemical data for use in atmospheric studies: evaluation Number 14; JPL Publication 02-25, National Aeronautics and Space Administration, Jet Propulsion Laboratory, California Institute of Technology, Pasadena, CA
146. Dobbs KD, Dixon DA, Komornicki A (1993) J Chem Phys 98:8852
147. Ma JB, Wu XN, Zhao YX, Ding XL, He SG (2010) Experimental and theoretical study of hydrogen atom abstraction from C_2H_6 and C_4H_{10} by zirconium oxide clusters anions. Chin J Chem Phys (submitted)
148. Ma YP, Ding XL, Zhao YX, He SG (2010) Chem Phys Chem. doi:10.1002/cphc.200900903
149. Zhao YX, Wu XN, Wang ZC, He SG, Ding XL (2010) Chem Commun. doi:10.1039/b924603g
150. Iwamoto M, Hlrata I, Matsukaml K, Kagawa S (1983) J Phys Chem 87:903
151. Ruszel M, Grzybowska B, Gąsior M, Samson K, Gressel I, Stoch J (2005) Catal Today 99:151
152. Tohver HT, Henderson B, Chen Y, Abraham MM (1972) Phys Rev B 5:3276
153. Ito T, Lunsford JH (1985) Nature 314:721
154. Nolan M, Watson GW (2005) Surf Sci 586:25
155. Rane VH, Chaudhari ST, Choudhary VR (2008) J Nat Gas Chem 17:313
156. Wang WG, Wang ZC, Yin S, He SG, Ge MF (2007) Chin J Chem Phys 20:412
157. Yin S, Ma YP, Du L, He SG, Ge MF (2008) Chin Sci Bull 53:3829
158. Döbler J, Pritzsche M, Sauer J (2005) J Am Chem Soc 127:10861
159. Goodrow A, Bell AT (2007) J Phys Chem C 111:14753